REPORT DOCUMENTATION PAGE

Form Approved
OMB NO. 0704-0188

1. AGENCY USE ONLY (Leave Blank)	2. REPORT DATE December 1999	3. REPORT TYPE AND DATES COVERED Final Report

4. TITLE AND SUBTITLE
URI Multidisciplinary Research Program for FY92-FY96 on Engine Combustion

5. FUNDING NUMBERS
DAAL03-92-G-0122

6. AUTHOR(S)
m. Corradini, P. Farrell, D. Foster, J. Ghandhi, J. Martin, R. Reitz, C. Rutland

7. PERFORMING ORGANIZATION NAME(S) AND ADDRESS(ES)
University of Wisconsin-Madison
Madison, WI 53706

8. PERFORMING ORGANIZATION
REPORT NUMBER

9. SPONSORING / MONITORING AGENCY NAME(S) AND ADDRESS(ES)
U. S. Army Research Office
P.O. Box 12211
Research Triangle Park, NC 27709-2211

10. SPONSORING / MONITORING
AGENCY REPORT NUMBER
ARO 30340.98-EG-URI

11. SUPPLEMENTARY NOTES
The views, opinions and/or findings contained in this report are those of the author(s) and should not be construed as an official Department of the Army position, policy or decision, unless so designated by other documentation.

12 a. DISTRIBUTION / AVAILABILITY STATEMENT
Approved for public release; distribution unlimited.

12 b. DISTRIBUTION CODE

13. ABSTRACT (Maximum 200 words)

The objectives of the Engine Research Center (ERC) are to conduct research leading to improved diesel engines, to provide trained manpower for U.S. needs, and to cooperate in technical information exchange with Army and other engine laboratories. Five projects were undertaken.

One project addressed using KIVA in conjunction with experimental work to produce a computational methodology for the design of new engines.

A second project worked to develop a physically based soot model for use in KIVA. The results of the model were compared with ERC generated data.

A third project aimed to produce a new combustion model for KIVA, which accurately portrays the physics of diesel ignition and heat release. The model is based on flamelet concepts which are enhanced by flame stretch and curvature, flame shortening, and turbulent diffusion. The model was compared to experimental data from the literature and from the ERC.

A fourth project involved experimentally measuring the liquid and vapor characteristics of very high pressure injectors under pressure and temperature conditions like those found in a diesel cylinder.

A fifth project worked to produce a new diagnostic system capable of characterizing a three-dimensional flow field in time. This project is still under development.

14. SUBJECT TERMS

...IBER OF PAGES

...CE CODE

17. SECURITY CLASSIFICATION OR REPORT	18. SECURITY CLASSIFICATION ON THIS PAGE	19. SECURITY CLASSIFICATION OF ABSTRACT	20. LIMITATION OF ABSTRACT
UNCLASSIFIED	UNCLASSIFIED	UNCLASSIFIED	UL

NSN 7540-01-280-5500

Standard Form 298 (Rev.2-89)
Prescribed by ANSI Std. 239-18
298-102

Table of Contents

TECHNICAL FINAL REPORT

1. ARO Proposal Number 30340-EG-URI

2. Period Covered by the Report: 1 January 1992 - 31 December 1997

3. Title of Proposal: URI Multidisciplinary Research Program for FY92-FY96 on Engine Combustion (No cost extension until 31 December 1997) Engine Research Center: Advanced Diesel Engine Research

4. Contract or Grant Number: DAAHL03-92-G-0122

5. Name of Institution: University of Wisconsin - Madison

6. Authors of the Report: Professors: M. Corradini, P. Farrell, D. Foster, J. Ghandhi, J. Martin, R. Reitz, C. Rutland

7. Manuscripts published (and accepted for publication) under ARO Sponsorship

Reitz, S-C Kong, and N.Ayoub, "Modeling Combustion in Compression Ignition Homogeneous Charge Engines" SAE 920512.

R.A. Booth and G.L. Borman, "Geometry of the Fuel Cloud Created by Impingement of a Diesel Fuel Jet onto a Small Heated Target," SAE 941950

D. Cleary and P.V. Farrell, "The Effects of Wall Temperature on Flame Structure During Flame Quenching", SAE 940683

M. Al-Roub, J. Naber and P.V. Farrell, "Heat Transfer for Single and Multiple Droplet Impingement on Walls", Proceedings of ICLASS '94, July 1994.

Rutland, C.J., Eckhause, J., Hampson, G., Hessel, R., Kong, S.-C., Patterson, M., Pierpont, D., Sweetland, P., Tow, T., and Reitz, R.D, "Toward Predictive Modeling of Diesel Engine Intake Flow, Combustion and Emissions," SAE 941897

R.J. Donohue, G.L. Borman and G.R. Bower, "Cylinder-Averaged Histories of Nitrogen Oxide in a D.I. Diesel with Simulated Turbocharging," SAE 942046

C.J. Rutland, N. Ayoub, Z.Han, G.Hampson, S.-C..Kong, K. Mather, D. Montgomery, M. Musculus, M. Patterson, D. Pierpoint, L. Ricart, P.Stephenson, and R.D. Reitz, "Diesel Engine Model Development and Experiments," 1995. SAE 951200, 1995 SAE Earth Moving Conference, April 4-5, Peoria, IL.

M. Al-Roub and P.V Farrell, "Droplet-Wall Impingement for Multiple Droplet Events," accepted for ASME Internal Combustion Engines Meeting, April 1995

T.F. Su, K. Goney, D. Schmidt, M. Corradini, and P.V. Farrell, "Cavitation in Diesel Fuel Injectors," submitted for 8th International Symposium on Multiphase Flow in Combustion, San Francisco, July 1995

David P. Schmidt, Tzay-Fa Su, Kayhan H. Goney, P.V. Farrell and M.L. Corradini. "Detection of Cavitation in Fuel Injector Nozzles." 8th ISTP Conference, San Francisco, July 1995.

D. Cleary and P.V. Farrell, "Single Surface Flame quenching Distance Dependence on Wall Temperature, Quenching Geometry, and Turbulence," SAE 950162

C.Y Choi, D.E. Foster, "In Cylinder Augmented Mixing Through Controlled Gaseous Jet Injection," SAE 952358

Nabil S. Ayoub, Rolf D. Reitz, "Multidimensional Modeling of Fuel Composition Effects on Combustion and Cold-Starting in Diesel Engines," SAE 95245

C.J. Rutland, N. Ayoub, Z. Han, G. Hampson, S.-C. Kong, D. Mather, M. Musculus, M. Patterson, L. Ricart, P. Stephenson, R.D. Reitz, "Progress Towards Diesel Combustion Modeling," SAE 952429

M. Al-Roub, J. Senda, and P.V. Farrell, "New-Wall Interaction in Spray Impingement", SAE Paper 960863

N.S. Ayoub, and R.D. Reitz, "Multidimensional Modeling of Fuel Composition Effects and Split Injections on Diesel Engine Cold-Starting." Accepted for publication. AIAA Journal of Propulsion and Power, 1996

Z. Han, R.D. Reitz, P.J. Claybaker, C.J. Rutland, "Modeling the Effects of Intake flow Structures on Fuel/Air Mixing in a Direct-Injected Spark-Ignition Engine." SAE 961192. 1996 International Spring Fuels and Lubricants Meeting, May 6-8. Dearborn, MI

Z. Han, R.D. Reitz, P.J. Claybaker, C.J. Rutland, J. Yang, and R.W. Anderson, "Modeling the Effects of Intake Flow Structures on Fuel/Air Mixing in a Direct-Injected Spark-Ignition Engine." SAE 961192 [SAME AS ABOVE?]

A.S. McLandress, R.G. Emerson, P.McDowell and C.J. Rutland, "Intake and In-Cylinder Flow Modeling Characterization of Mixing and Comparison with Flow Bench Results," SAE 960635, 1996 SAE International Congress, Feb 26-29

L.M. Ricart, and R.D. Reitz, "Visualization and Modeling of Pilot Injection and Combustion in Diesel Engines," SAE 960833, 1996

H.E. Snyder, And R.D Reitz, "Gas Efficient Liquid Atomization Using Micro-machined Spray Nozzles," SAE 960859, 1996.

Snyder, H.E., and Reitz, R.D.,"Gas Efficient Liquid Atomization Using Micro-machined Spray Nozzles," SAE Paper 960859, SAE Transactions, Vol. 105, Section 3, Journal of Engines, pp. 1260-1270, 1996.

Ricart, L.M., and Reitz, R.D., "Visualization and Modeling of Pilot Injection and Combustion in Diesel Engines," SAE Paper 960833, SAE Transactions, Vol. 105, Section 3, Journal of Engines, pp. 1164-1183, 1996.

Al-Roub M., Senda J. and Farrell, P. ."Near-Wall Interaction in Spray Impingement", SAE Paper 960863,

Su, T., Warrick,. C. and Farrell, P., "Temperature Effects On High Pressure Sprays", SAE 962005, 1996.

Ayoub, N.S., and Reitz, R.D., "Multidimensional Modeling of Fuel Composition Effects and Split Injections on Diesel Engine Cold-starting," AIAA Journal of Propulsion and Power, Vol. 13, pp. 123-130, 1997.

Senecal, P.K., Xin, J., and Reitz, R.D., "Pedictions of Residual Gas Fraction in IC Engines," SAE Paper 962052, SAE Transactions, Vol. 105, Section 3, Journal of Engines, pp. 2243-2254, 1996.

Choi, C., Bower, G., and Reitz, R.D., "Effects of Biodiesel Blended Fuels and Multiple Injections on DI Diesel Engine Emissions, SAE Paper 970218, Accepted for SAE Transactions, 1997.

Ricart, L.M., Xin, J., Bower, G.R., and Reitz, R.D., "In-Cylinder Measurement and Modeling of Liquid Fuel Spray Penetration in a Heavy-Duty Diesel Engine," SAE Paper 971591, Submitted for SAE Transactions, 1997.

Senecal, P.K., Uludogan, A., and Reitz, R.D., "Development of Novel Direct-Injection Diesel Engine Combustion Chamber Designs using Computational Fluid Dynamics", SAE Paper 971594, Submitted for SAE Transactions, 1997.

Al-Roub and Farrell, P., "Atomization of Thin Liquid Films by Droplet Impact", Atomization and Sprays 7, p. 531, 1997.

Mislevy, S. and Farrell, P., "Wall Impingement Spray Characteristics", ICLASS '97, August 1997

Snyder, H.E., and Reitz, R.D., "Direct Droplet Production from a Liquid Film: A New Gas-Assisted Atomization Mechanism," Accepted, Journal of Fluid Mechanics, 1998.

Stanton, D.W., Senecal, P.K., Hung, C.C., Rutland, C.J., Reitz, R.D., "Methodology for Model Discrimination and Criticism for Liquid Atomization Data," Accepted for publication, Atomization and Sprays, 1998.

Xin, J., Ricart, L., and Reitz, R.D., "Computer Modeling of Diesel Spray Atomization and Combustion," Accepted for publication, Combustion Science and Technology, 1997.

Mislevy, S. and Farrell, P., "Spray Characteristics of a Diesel Fuel Spray Impinged on a Raised Surface", ILASS-Europe , July 1998

Al-Roub, M. and Farrell, P., "Heat Transfer for Impinging Drops", submitted to Journal of Heat Transfer

8a. Degrees Awarded and Theses Published (under ARO Sponsorship)

1994

Booth, Richard, MS
Investigation Of Impinging Diesel Spary Hydrodynamics And Heat Transfer

Cleary, David, PhD
An Experimental Investigation Of Single-Surface Flame Quenching

Eckhouse, Joel, MS
Modeling Spray Wall Impingement Heat Transfer On Direct Injection Engines

1995

Ayoub, Nabil, PhD
Modeling Multicomponent Fuel Sprays In Engines With Application To Diesel Cold-Starting

Boucher, Stephen E., MS
Preliminary Study Of A Shear Plane Layer Formed Between Two Parallel Flows.

Choi, Cathy, MS
In Cylinder Augmented Mixing Through Controlled Gaseous Jet Injection

Claybaker, Peter, MS
Streamlined Production Of Engine Meshes For Kiva-3

Krause, Steven F., MS
The Effect Of Intake Port Geometry On In-Cylinder Fluid Motion In A Reciprocating I.C. Engine.

Lee, Laurence, MS
Oil Film Thickness Between Top Piston Ring And Engine Liner Near Ring Reversal Of A Single Cylinder S.I. Engine.

McLandress, Andrew, MS
Intake Flow Mixing And Characterization For Diesel Simulations

Mehri, Darius, MS
The Design Of A High Pressure, High Temperature Turbulent Mixing Layer Apparatus

Ricart, Laura M., MS
The Effects Of Heat Transfer And Mixing On Diesel Ignition And Combustion

Stanton, Donald W., MS
Modeling Fuel Film Formation And Wall Interaction In Diesel Engines.

1996

Al-Roub, Marwan Abu, Phd
Hydrodynamics And Heat Transfer Of Multiple Droplet Impingement

Ducu, Dan O., PhD
Calibration Of The Laser Induced Fluorescence Technique Applied To Oil Film Thickness Measurements On A Diesel Engine Cylinder Liner By Using Capacitance Gauges

Emerson, Roy, MS
Intake Flow Modeling In KIVA-3 And Comparison With Experiments

Pardyjak, Eric R., MS

Development And Evaluation Of Turbulent Mixing Models

Raney, Helen E., MS
Analyzing Cycle To Cycle Variations In The Intake Flow Using A Water Analog Engine

Warrick, Charles B., MS
Design And Testing Of A High Temperature, Engine-Fed Combustion Chamber For Multi-Hole Fuel Spray Analysis

1997

Senecal, Peter Kelly
Exploring Alternatives to Conventional Di Diesel Combustion Systems Using Computational Fluid Dynamics

Schmidt, David P.
Cavitation in Diesel Fuel Injector Nozzles

Donahue, Richard PhD
Experimental Studies on Ring Pack Design Parameters and The Analysis of Radial Ring Collapse.

1998

Ricart, Laura, PhD
An Experimental and Computational Study of Fuel Injection, Mixing and Combustion in Diesel Engines

PEOPLE WHO HAVE BEEN SUPPORTED ON THE GRANT BUT WHO HAVE NOT YET COMPLETED THESIS:

Calvin Hung, Kevin Sholes, Todd Rose, Scott Mislevy, Taewoong Hwang, Robert Borthwick, Yoshi Ieda, Robert Vets (Terminated)

STATEMENT OF THE PROBLEM STUDIED

The objectives of the Engine Research Center (ERC) are to conduct research leading to improved diesel engines, to provide trained manpower for U.S. needs, and to cooperate in technical information exchange with Army and other engine laboratories. Five projects undertaken to meet these objectives; they are summarized below.

The objective of the first project was to combine the use of KIVA and some limited experimental work to produce a methodology for the design of new engine concepts using computational techniques. This methodology was developed using KIVA and cycle analysis applied to the problem of producing a high power-to-weight ratio engine that burns JP8 fuel and is suitable for use as an army gen-set powerplant.

The objective of the second project was to develop a physically based soot model for use in KIVA and to compare results from this model with data from engines being run in the ERC. These data include in-cylinder soot measurements on a Cummins turbocharged NH and a Caterpillar engine with very high pressure injection. The model will be combined with the advanced combustion model of Project 3.

The objective of the third project was to produce a new combustion model for KIVA, which will more accurately portray the physics of diesel ignition and heat release. The model was based on flamelet concepts enhanced by inclusion of flame stretch and curvature, flame shortening, and turbulent diffusion. Adjustments and model parameter sensitivity tests were performed by comparisons to ERC engine data and off-engine data from the existing literature.

The objective of the fourth project was to experimentally measure the liquid and vapor characteristics for very high pressure injectors under pressure and temperature conditions like those found in a diesel cylinder. Techniques of phase doppler particle analysis, and droplet sizing and image velocimetry were applied to advanced design injectors which inject into an engine-fed-bomb having very good optical access. The bomb duplicates the central injection and bowl geometry of a modern diesel engine. The resulting were compared with KIVA computations.

The objective of the fifth project is to produce a new diagnostic system capable of characterizing a three dimensional flow field in time. This diagnostic is to be applied to a see-through engine and should allow balances to be applied to a control volume within the cylinder. Such balances are a very important step in understanding transient 3-D flows and should be of great help in validating the KIVA flow models.

In the paragraphs below the results are presented as three separate sub-reports. Work toward the fourth and fifth objectives was integrated into the results used in the development and validation of results for the first three objectives.

SUMMARY OF RESEARCH FINDINGS

COMPUTATIONAL METHODOLOGY FOR ENGINE DESIGN

The goal of this project was to explore methods to incorporate the use of multidimensional modeling in the engine design process. Traditionally, engine design has been done using experimental trial and error and experience, coupled with cycle analysis. However, new tools such as comprehensive computer models are now available. This project aims to develop a methodology for engine combustion chamber design by using advanced computer models guided by informative experiments.

The approach used was to apply computer models to explore specific engine design concepts. Emphasis was placed on developing methods to analyze the in-cylinder flow predictions in order to explain trends and suggest improved design configurations. The first engine concept was one studied previously under TACOM funding at the ERC in which the fuel spray is targeted to impinge on a raised center-body or pedestal on the piston. This engine concept was shown to produce a well-atomized and dispersed fuel cloud which could be spark-ignited with very low cetane number fuels. The second engine concept exploited the use of multiple injectors to help disperse the spray droplets and to enhance the fuel-air mixing. In order to verify the model results and to help establish engine geometry design parameters, specially designed experiments were performed for the impingement engine concept.

Experimental Analysis of Spray and Engine Geometry Design Parameters

Booth [1] conducted a comprehensive investigation of fuel spray impingement in a high-pressure ambient temperature spray chamber, where the fuel was impinged onto a raised target. The injection parameters were set at levels equivalent to that found in small utility diesel engines with fuel quantities of approximately 20 mg/injection. The study had three main parts. First, a laser interrupt method was used to determine the radial penetration of the impinged spray for a large number of variables in order to investigate the effects of many engine geometry/fuel injection system design parameters. Second, a series of high-speed films were taken to verify the penetration data from the laser interrupt method. Lastly, an experiment was performed to determine the heat transfer from a heated target to the impinging spray. This work was conducted in a high-pressure spray chamber and no drop sizing was conducted at that time.

For the laser interrupt study, a large number of variables were selected. In order to see which of the many parameters had a significant effect on penetration, a fraction factorial design was used as a part of a developmental method for the analysis of such engine/spray parameters. This design allowed a large number of variables to be studied with a relatively small number of runs. The laser interrupt method only provided penetration time at fixed distances, which were set to 10, 15, 20, and 30 mm from the spray centerline. The results showed that two important variables were ambient density and target diameter. As the ambient density, ambient pressure, and target diameter increased, the penetration time increased. In other words, the spray did not penetrate as fast. This effect of ambient density has also been seen with free sprays and impingement on flat plates. In regards to the effect of target diameter, for the smaller target the spray began to entrain air closer to the impingement point where the velocity was high. The increased air entrainment caused more momentum exchange with the gas and thus lower penetration. The target temperature, target material, and fuel type had an insignificant effect on penetration time. In addition, impingement distance had little effect when the penetration time was taken from the time of impingement.

Next, based on the above results, high-speed films of the spray development were taken for 10 test cases. The penetration proceeded quickly at first, then slowed down in the later stages of the injection. In looking at the spray penetration, higher ambient density and smaller target diameters resulted in lower penetration, which was also seen from the laser interrupt results. However, no effect of fuel type or target temperature was found. One problem was that effects due to gas density gradients around the target made spray development impossible to see until after impingement and the spray had passed the boundary layer temperature gradients, thus making it difficult to determine impingement times. Since the heat transfer results showed that the heat transferred into the spray was not enough to significantly vaporize the spray in any of the cases, future impingement work would utilize both a different visualization scheme and non-heated targets.

Mislevy's [2] work examined the behavior of a non-vaporizing diesel fuel spray impinging on a raised surface on the piston crown in a motored engine. Booth's work was used as a guideline in order to do a more detailed investigation on what appeared to be the most important engine geometry design parameters. For the spray visualization, a laser light sheet was created with an Argon-ion laser in order to illuminate a plane of the spray. An acousto-optic modulator in conjunction with an iris were used to act as an electronic shutter, and the spray was imaged onto 35 mm film with the camera positioned at 90° to the light sheet. Once injection was initiated, the third injection event in the series was captured on film and each image represented a separate injection event. In contrast to the back illumination scheme used by Booth, this method would allow for more information on the internal spray structure. An atmospheric spray chamber was built, and this new illumination scheme was tested for a variety of impingement target diameters, heights, and impingement distances. This scheme revealed that under atmospheric conditions, the post-impingement spray showed a distinct separation between (1) a vortex region forming on the edge of the target and (2) what appeared to be bigger drops that are unaffected by the vortex and penetrate outward at small angles of incidence. These details are seen in Figure 1a.

These larger drops were not seen in Booth's work, which used a different imaging scheme and was also at higher ambient gas pressures, as summarized in Figure 2. Therefore, the laser sheet imaging scheme was next used in a high pressure bomb, with varying ambient pressure and density. Larger drops were identifiable for the low-density cases for ambient pressures up to 1.7MPa. However, as the ambient density was increased to engine-like values, only the large vortex region was seen. At this time, it is still unclear as to whether the bigger drops are a result of post-impingement spray coalescence or droplet splashing of the fuel film that may be on the pedestal from a previous injection.

Next, a single cylinder, optical access research engine was modified for direct fuel injection and the impingement targets were bolted to the piston top. A 30 mm high acrylic annulus was placed between the cylinder block and head to allow optical access, as shown in Figure 1b. This height of the annulus was used for increased optical access as well as to provide the capability to test a range of impingement distances and target heights. A compressed air intake system was added to boost the intake pressure in order to simulate higher compression ratios. As with the spray chamber results, when the penetration time is taken from the time of impingement, neither impingement distance nor pedestal height had a major impact on spray penetration. In addition, boosted intake pressures and thus higher density at TDC showed less penetration. Although this was not unexpected, based on the spray chamber results, Mislevy's results have moved a step further and include the effect of piston motion, which causes continual movement of the spray pedestal as well as effects the bulk motion of the in-cylinder flow.

In Mislevy's work the Phase Doppler Particle Anemometer (PDPA) has been employed to get information regarding post-impingement spray drop velocities and sizes in the atmospheric spray chamber and in the motored engine. This information is invaluable for refinement of the impingement models.

Modeling Spray and Engine Geometry Design Parameters

In an effort to develop a computational methodology for engine design, a multi-dimensional CFD code, based on the KIVA code, was used to examine several unconventional diesel engine concepts. Two of these concepts, referred to as SIMPLE and MICS are shown in Figure. 3. While the MICS combustion chamber geometry is the same as the baseline Caterpillar engine, the chamber geometry for the SIMPLE engine is similar to the pedestal engine of the motored impingement experiments of Mislevy [1]. In the SIMPLE concept all of the fuel is injected vertically downward onto the centrally located pedestal which produces an azimuthally uniform fuel/air mixture. In addition to the engine case, injection conditions were chosen to replicate the experimental impingement conditions for code validation. In the MICS concept, multiple injectors are used to enhance the gas-phase swirl motion and to increase the surface area for fuel/air mixing. Additional concepts referred to as the GAMMA and WHEEL engines were also investigated and details can be found in Senecal's papers [3, 4].

The SIMPLE design concept utilizes a centrally located impingement pedestal to enhance atomization and provide fuel in the center of the combustion chamber. In order to assess the capability of the multi-dimensional models for simulating this type of forced spray/wall impingement, comparisons were first made with the non-vaporizing spray bomb experiments of Naber [5], Booth [1] and Mislevy [2]. While these comparisons focused on the overall structure and penetration of the fuel spray (e.g., Fig. 1(c)), continuing work will compare drop sizes and velocities for the post–impingement spray. Figure 1(d) presents the computed spray drop distribution for one of Booth's cases at approximately 2 ms after the start of injection. The major features of the impinged spray are evident in this figure. While the larger drops (indicated by dark grey) penetrate to the front of the spray, the smaller drops (indicated by light grey) are "caught up" in the spray-induced vortices existing both above and below the pedestal. This is seen in the experimental images shown in Figures 1(a) and 1(b). Figure 2 shows the liquid spray tip penetration for this case as functions of time as measured by Booth and as calculated with the present KIVA code. As can be seen the agreement is excellent. Further comparisons with spray/wall impingement experiments can be found in [6] for the experiments of both Naber and Booth.

With this and other validation studies completed, the code was next applied to engine cases. The resulting soot/NOx points and soot/isfc points for the various concepts and the baseline heavy-duty diesel engine for an SOI of -9 deg. atdc are shown in Figure 4. It was found that for the given speed and load (1600 rpm, 75% load), particular engine design parameters had a large impact on the resulting emissions for each concept. For example, as shown in the figure, the gas-phase swirl level has a significant effect on the

engine-out soot emissions for the SIMPLE engine due to the resulting flow field in the spray-axis plane. The soot/NOx points for this concept are shown in Figure 4(a) for a swirl level of one (SIMPLE-1) and zero (SIMPLE-0). While the SIMPLE-1 case produces a flow field which inhibits all or most of the fuel from penetrating deep into the piston bowl resulting in delayed burning, in the SIMPLE-0 case the fuel leaving the pedestal is directed down into the bowl by a counterclockwise vortex set up by the squish flow.

The present results suggest that in the SIMPLE design the fuel spreads from the pedestal in an axisymmetric fashion and is forced down into the bowl (in the case of zero swirl). The relatively low NOx values can be attributed to the longer ignition delay which is due to the distance the large drops need to travel before they impact on the pedestal and break up to form a fuel/air mixture. These large drops do not vaporize significantly prior to impingement. As a result, the NO reduction mechanism associated with pedestal impingement seems to be similar to that of retarding the injection timing, which was also shown to be the case by Han et al. [7] for certain multiple injection schemes. Note, however, that the increased soot that typically accompanies retarded injection timings in the conventional design is not a problem with the present concept because of the enhanced fuel/air mixing characteristic of the design.

When multiple injectors were used in the MICS cases, the results show that the number of injectors, and hence the number of nozzle holes per injector, had a large effect on the production of emissions. In the MICS-2 concept, the use of two three-holed injectors produced locally fuel-rich regions, and thus high soot levels, due to the close spacing between the fuel sprays. As a result, three two-holed injectors were used in the MICS-3a case to reduce the extent of the fuel rich regions, however, the enhanced burning rate resulted in higher in-cylinder temperatures and hence, higher NOx levels. It was found that the burning rate could be controlled by reducing the angle between the sprays, as in the MICS-3b case, resulting in both lower soot and NOx when compared to the baseline case.

Engine Design Methodology

In the present study experiments were used to both validate the models and to help select engine geometries for computational investigation. Once a "baseline" configuration was selected for a particular concept, the models were used to gain experience about how changing certain parameters affected the performance of the design. The models were then used to optimize the engine design parameters for minimum emissions and fuel consumption. Engine performance was monitored by correlating predicted engine-out emissions with those in-cylinder flow details that were found to significantly influence emission formation rates. For example, tracking the percentage of the total cylinder gas mass which is at a high temperature was found to be a useful measure of the NOx formation potential for each particular engine design concept.

Similarly, the percentage of the charge with rich equivalence ratios was found to be an excellent predictor of the sooting potential for each engine design concept. In addition, design modifications (such as orienting the injection toward the squish flows, optimizing the interactions between spray plumes or exploiting swirl) were suggested to move soot-producing regions toward oxygen-rich regions within the combustion chamber to promote fuel and soot oxidation. The magnitude and timing of peak cylinder pressure, and the burned fuel histories were found to influence isfc and emissions. These criteria were used as indicators to suggest parameter variations, such as the number of injector holes, or the injector orientation, so as to minimize emissions and fuel consumption. Additional details of the methodology used to find optimal design criteria can be found in [3, 4 and 6].

References

1. Booth, R.A., "Investigation of Impinged Diesel Spray Hydrodynamics and Heat Transfer", MS Thesis, Dept. of Mechanical Engineering, University of Wisconsin-Madison, 1994.
2. Mislevy, S.P. and Farrell, P.V., Spray Characteristics of an Impinged Diesel Fuel Spray," The 7th International Conference on Liquid Atomization and Spray Systems (ICLASS '97), Seoul, South Korea, August 1997.
3. Senecal, P.K., Uludogan, A., and Reitz, R.D., "Development of Novel Direct-Injection Diesel Engine Combustion Chamber Designs using Computational Fluid Dynamics," SAE 971594, 1997.
4. Senecal, P.K., Uludogan, A., and Reitz, R.D., "Exploring Alternatives to Conventional DI Diesel Combustion Systems using Multi-Dimensional Spray and Combustion Modeling," ASME 97-ICE-55, 29-2, 1997.
5. Naber, J., Enright, B. and Farrell, P., "Fuel Impingement in a Direct Injection Diesel Engine," SAE 881316, 1988.
6. Senecal, P.K., "Exploring Alternatives to Conventional DI Diesel Combustion Systems using Computational Fluid Dynamics," MS Thesis, Dept. of Mechanical Engineering, University of Wisconsin-Madison, 1997.
7. Han, Z., Uludogan, A., Hampson, G.J. and Reitz, R.D., "Mechanism of Soot and NOx Emissions Reduction using Multiple-Injection in a Diesel Engine," SAE 960633, 1996.

a) atmospheric spray chamber.

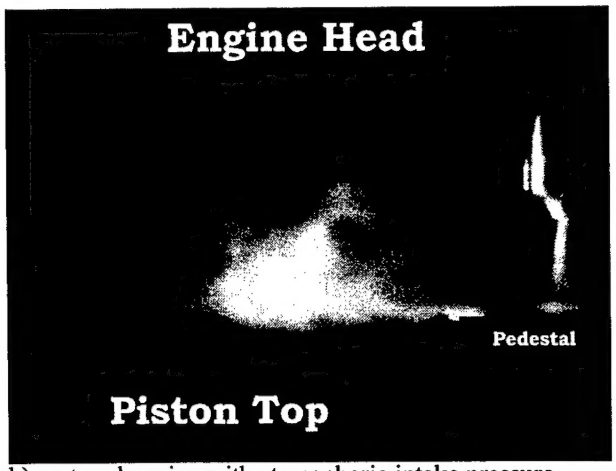

b) motored engine with atmospheric intake pressure

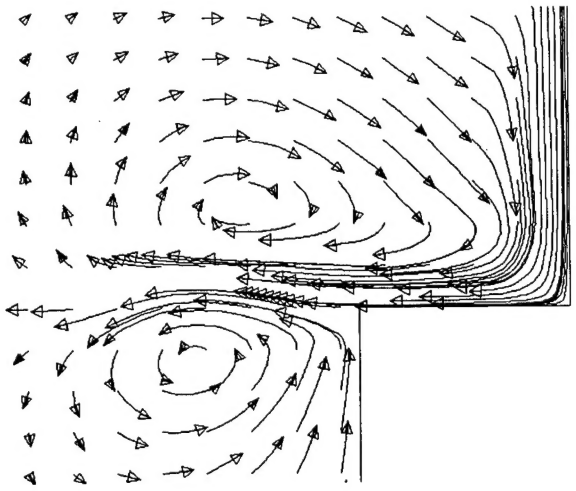

c) Vector plot of KIVA results.

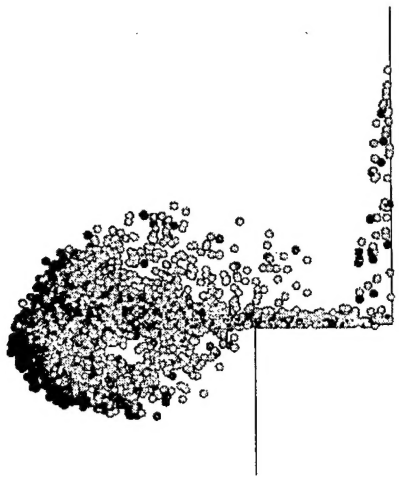

d) Computed spray drop distribution from KIVA.

Figure 1. Comparison between experimental photographs of impinging spray and KIVA results for 2.3 ms after impingement.

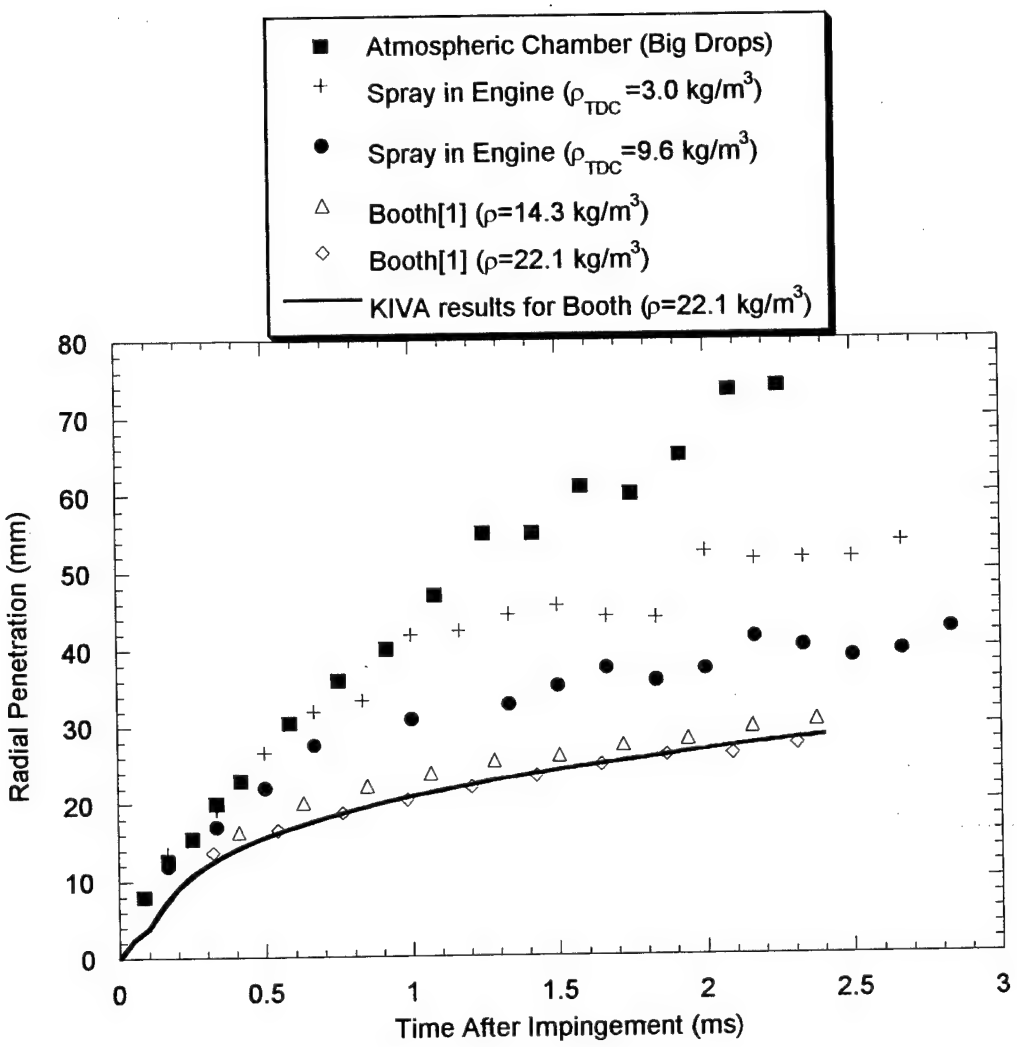

Figure 2. Comparison of spray penetration in motored engine, atmospheric pressure chamber, and high pressure spray chamber results.

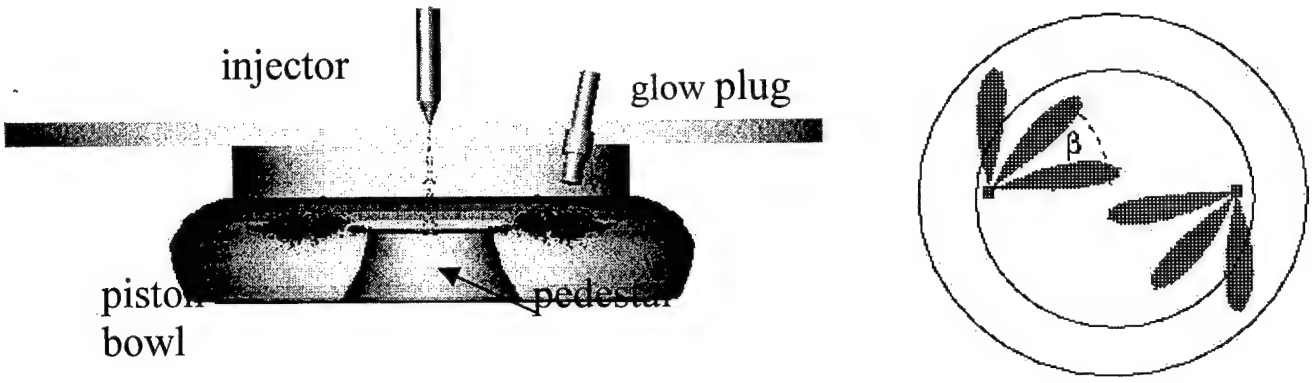

(a) (b)

Figure 3: Schematics of the (a) SIMPLE combustion chamber geometry (glow plug was not considered in the present work) and (b) MICS-2 injection scheme.

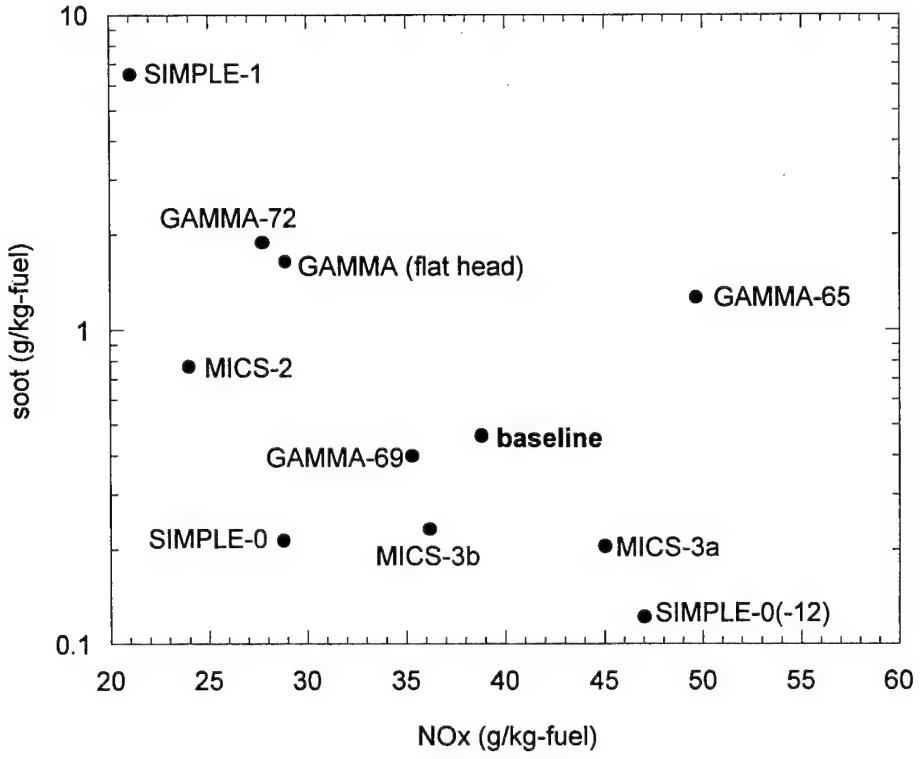

Figure 4: (a)Soot/NOx tradeoff points for the various concepts for an SOI of -9 deg. atdc.

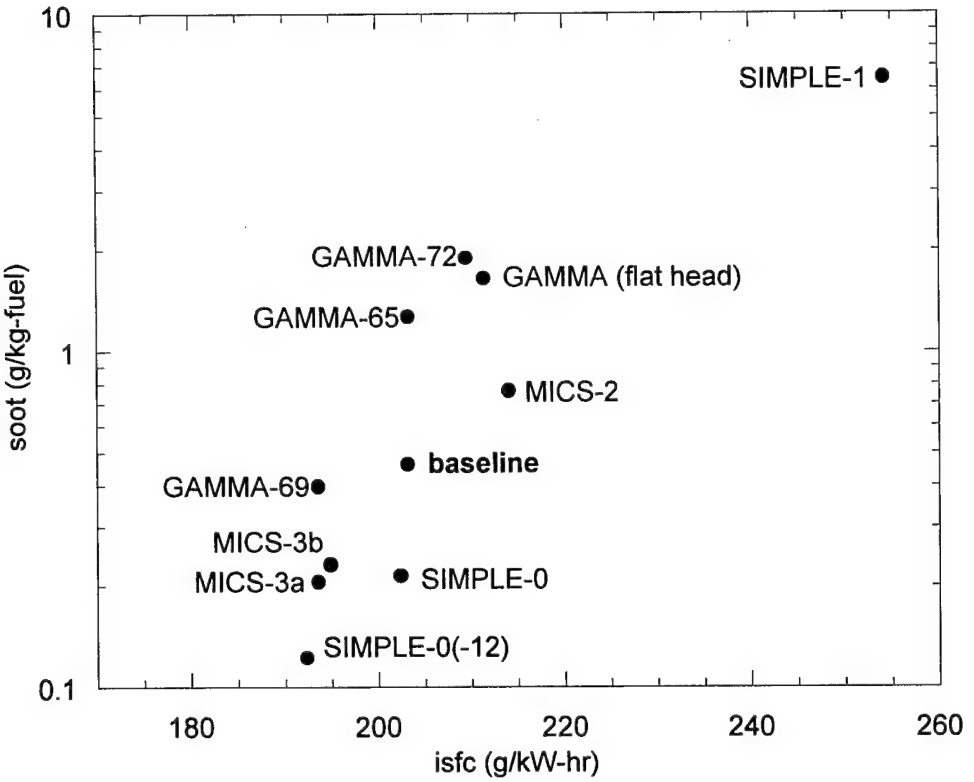

Figure 4: (b) soot/isfc points for the various concepts for an SOI of -9 deg. atdc.

DEVELOPMENT OF A MULTI-STEP PHENOMENOLOGICAL SOOT MODEL

Nomenclature:

Roman symbols:

- a - stoichiometric coefficient in reaction (1);
- A_i - preexponential factor for the Arrhenius rate coefficient of the ith process;
- b - stoichiometric coefficient in reaction (2);
- d_p - soot particle diameter;
- E_i - activation energy for the Arrhenius rate coefficient of the ith process;
- f_v - soot volume fraction;
- I_{sct} - intensity of scattering signal;
- I_{rad} - intensity of radiation signal;
- k - turbulent kinetic energy;
- k_B - Boltzmann constant;
- $k$ext - extinction coefficient;
- n_C^{GR} - number of carbon atoms in growth species;
- Kn - soot particle Knudsen number;
- N - soot particle number density;
- N_A - Avogadro's number;
- $P(\lambda,T)$ the Plank's function;
- Q_{sca} - volumetric scattering cross-section;
- r_i - the ith reaction rate;
- r_i^{kin} - kinetic rate of the ith process;
- r_i^{mix} - mixing rate of the ith process;
- S - soot surface area;
- t - reaction time;

T - the temperature;
w_C - molar weight of a carbon atom;
w_f - molar weight of fuel;
w_{GR} - molar weight of growth molecule;
w_{PR} - molar weight of precursor species;
y_f - mass fraction of fuel;
y_{GR} - mass fraction of growth species;
y_{PR} - mass fraction of precursor species;
y_S - soot mass fraction;

Greek symbols:
α - van der Waals enhancement factor of soot coagulation rate;
α_S - calibration constant in Eq. (25);
α_r - calibration constant in Eq. (26);
β - soot particle collision frequency;
β_{fm} - soot particle collision frequency in the free molecular regime;
β_{nc} - soot particle collision frequency in the near-continuum regime;
ε - rate of dissipation of turbulent kinetic energy;
λ - light wavelength;
μ - molecular viscosity;
ρ - mixture mass density;
ρ_S - mass density of soot particle material;
ϕ - equivalence ratio.

Introduction

Particulate emissions represent one of the most deleterious pollutants generated during Diesel combustion. The newly suggested Environmental Protection Agency (EPA) standards impose very strict regulations on particulate levels with specific emphasis on the size of emitted particles [1]. According to the recent epidemiological studies, particles two and one half microns or less in diameter may be the most harmful because they penetrate deep into lung tissue. The new standards have resulted in increased interest in fundamental understanding of the mechanisms of soot particle formation and oxidation in internal combustion engines.

Multidimensional computer simulations are becoming an essential part of the modern engine design process [2]. The ability to predict soot formation is one of the key elements needed to assist in the optimization of engine performance with respect to the emission levels. Among the many directions of research, there is a pressing need for practical computer models that would be able to describe the process of soot formation during Diesel combustion on both qualitative and reasonably quantitative levels.

Prediction of soot formation and oxidation has always been one of the biggest challenges in combustion modeling [3,4]. A variety of different soot models ranging from simple empirical correlations relating the amount of particulates in the exhaust to the engine operating parameters [5] to very detailed descriptions of pre-particle chemistry and soot particle dynamics [6-9] have been proposed for engine simulations. While the empirical correlations offer simplicity and computational efficiency, they cannot be applied reliably to the systems other than those for which they were specifically calibrated. In addition, these models provide very limited insight to the soot formation process in the system under consideration. Detailed models, on the other hand, treat the process of soot formation in considerable detail and are becoming nearly quantitative for simple combustion systems [10-13]. Yet, these models are usually not considered for the use in engine or three-dimensional CFD modeling in general since they are very expensive computationally. At present, however, with the development of efficient methods of reaction mechanism reduction and increased speed of modern computers, the application of detailed models is becoming more feasible. Nevertheless, there is still a number of problems that prevent us from the immediate use of these models in routine practical engine simulations. First, these models require the explicit knowledge of the comprehensive reaction mechanisms describing fuel pyrolysis and oxidation under engine conditions. Such mechanisms are normally very complex and not readily available for multicomponent blends of practical Diesel fuels; the majority of the current efforts was focused on relatively simple hydrocarbon fuels such as natural gas [6] or n-heptane [7,8]. Furthermore, the submechanisms describing formation of polycyclic aromatic hydrocarbons (PAH) widely regarded as soot particle precursors, and therefore needed for the description of pre-particle chemistry, are still the subject of uncertainty [14,15]. The other problem is the accurate representation of interactions between the detailed chemistry and turbulent mixing on a subgrid level. Pitsch et al. suggested the approach based on a representative interactive flamelet concept that was applied successfully to a high-pressure spray bomb [7,16] and a VW direct-injection Diesel engine [8] combustion. However, this model is very demanding in terms of computational time and still requires further validation. Finally and perhaps most importantly for practical applications, the predictions of soot formation and oxidation in an engine are extremely sensitive not only to the choice of soot model itself but also to the other submodels needed to describe the complex process of Diesel combustion such as the turbulence model and particularly the fuel spray model [17,18]. The existing uncertainties in these models can essentially eliminate the advantages of using a detailed kinetic treatment of soot formation in practical engine simulations.

In this work, we adopt a compromise approach and use a phenomenological model of soot formation and oxidation. Phenomenological or semi-empirical kinetic models of soot formation have a long history of development and use from

the early works of Tesner and co-workers [19] to many recent computational efforts [20-23]. It is worthwhile to point out that, facing the uncertainties in soot chemistry, some authors have applied semi-empirical models of soot formation even to simple laminar flame systems when the detailed description of fuel chemistry was available [20]. Semi-empirical models describe the complex process of soot formation and oxidation in terms of several global steps. Such an approach is particularly advantageous for the practical combustion simulations. On one hand, a simple system with a well-defined kinetic behavior is substantially easier to interpret and to calibrate for the operation conditions of interest. On the other hand, once properly calibrated, the model is expected to behave reasonably within a certain range of operating conditions describing the qualitative trends and even providing semi-quantitative predictions since it captures the basic fundamental features of the process of soot formation and oxidation.

One of the most popular semi-empirical models of soot formation in a Diesel engine suggested by Hiroyasu and Kadota [24] includes only two steps: (1) soot formation linked directly to the concentration of initial fuel; and (2) soot oxidation related to the concentration of molecular oxygen. This model and its modifications were successfully applied in a number of studies [25,26]. However, it was also shown that two-step models have rather limited range of applicability [27]. In addition, these models do not provide the information regarding the size of soot particles which, as it was mentioned above, is one of the issues of practical interest. Therefore, higher-level, multi-step semi-empirical models of soot formation are currently considered [27-30]. Belardini and co-workers [27-29] demonstrated the reasonable agreement between the predictions of their multi-step model and experimental data obtained for a number of test cases using different fuels and injection timings. Fusco et al. [30] indicated the consistency of the trends reported in the literature and the predictions of their model.

In the present work, a modified version of the phenomenological model suggested by Fusco et al. [30] was implemented and validated against the experimental data derived from the in-cylinder soot optical measurements in a single-cylinder DI Diesel engine.

Model Formulation

The computations were performed using the KIVA-II code [31] enhanced with the submodels developed at the Engine Research Center of the University of Wisconsin-Madison [32]. The specific improvements particularly relevant to the present study include RNG k-ε turbulence model [33], the Shell 5-species autoignition kinetic model [34,35], characteristic-time combustion model [36,37], and spray atomization model accounting for combined Kelvin-Helmholtz and Rayleigh-Taylor droplet instabilities [18].

The basic structure of the soot model used in the present study was taken from the work of Fusco et al. [30] with modifications that will be discussed later in the paper. The model incorporates, via global rate expressions, the physical processes of fuel pyrolysis and soot particle inception, surface growth, coagulation and oxidation. These processes are shown schematically in Fig. 1.

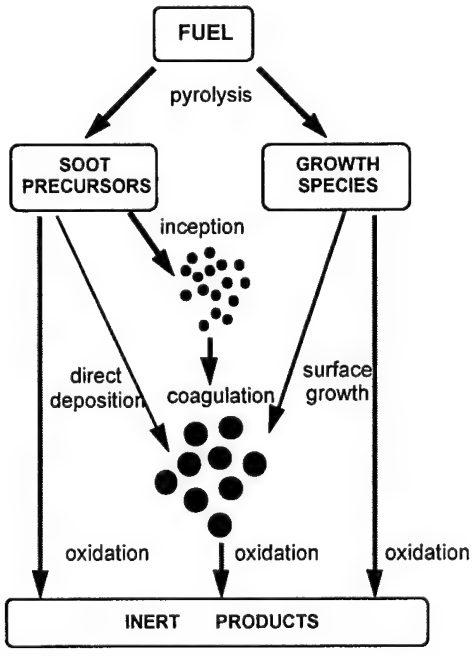

Figure 1. Structure of the phenomenological model of soot formation and oxidation.

The pre-particle chemistry is represented by pyrolytic decomposition of fuel forming generic soot particle precursor (PR) and growth (GR) species. Both processes are described with single-step global kinetic reactions:

$$\text{Fuel} \rightarrow a\ \text{PR} + \text{products} \qquad (1)$$

$$\text{Fuel} \rightarrow b\ \text{GR} + \text{products} \qquad (2)$$

where the stoichiometric coefficients *a* and *b* are chosen to preserve the carbon balance in reactions (1) and (2). It should be pointed out that, in many similar semi-empirical models, the formation of precursors is usually related to the growth species commonly assumed to be acetylene, C_2H_2, rather than to the parent fuel itself. Such an approach may be reasonable for the combustion of small hydrocarbons when formation of the first aromatic ring proceeds through acetylene or its derivatives. A typical Diesel fuel, however, normally contains a significant amount of aromatics. The formation and growth of polycyclic aromatic hydrocarbons (PAH) widely regarded as soot particle precursors may occur differently and be closely linked to the concentration of parent fuel as assumed in the present model.

Soot particle inception proceeds via conversion of precursor species into incipient soot particles,

$$\text{PR} \rightarrow \text{soot.} \qquad (3)$$

Soot particles undergo further growth by surface reaction with the growth species,

$$\text{soot} + \text{GR} \rightarrow \text{"bigger soot"} + \text{products} \qquad (4)$$

and particle-particle coagulation,

$$\text{soot} + \text{soot} \rightarrow \text{"bigger soot"} \qquad (5)$$

All model species, i.e., PR, GR, and soot are also subjected to oxidation, with the rates assumed to be related to concentration of molecular oxygen:

$$\text{PR} + O_2 \rightarrow 2\ \text{CO} + \text{products} \qquad (6)$$

$$\text{GR} + O_2 \rightarrow 2\ \text{CO} + \text{products} \qquad (7)$$

$$\text{soot} + O_2 \rightarrow \text{"smaller" soot} + 2\ \text{CO} + \text{products.} \qquad (8)$$

For simplicity, the soot particle size distribution is assumed to be monodisperse locally, however, the particle size can be different at different locations inside the cylinder (different computational cells). This assumption, although common for most semi-empirical models [19-23, 27-30] and even some detailed models [7,8], is obviously not valid if the local soot particle size distribution is wide. Such a situation usually takes place when fast nucleation rates, caused by high concentration of precursors, occur simultaneously with high rates of surface growth: a continuous supply of small incipient particles and the rapid growth of already existing particles result in the spread of particle size distribution. This problem can be at least partially corrected by including another process into the kinetic model - direct deposition of precursor species onto the soot particle surface:

$$\text{soot} + \text{PR} \rightarrow \text{"bigger" soot.} \qquad (9)$$

Inclusion of process (9) is justifiable physically since large PAH molecules regarded as soot particle precursors are believed to contribute to soot surface growth directly [38], and the direct deposition of PAH on soot surface is included in most detailed models [7, 8, 10-13]. On the other hand, the process (9) also helps to avoid problems with wide particle size distributions. If mature soot particles are present in the system, they will consume PR via reaction (9) preventing the generation of small incipient particles and, therefore, the expansion of the particle size distribution.

Based on the model processes outlined by Eqs. (1)-(9), the model rate equations are written as follows:

$$\frac{dy_{\text{PR}}}{dt} = a\frac{w_{\text{PR}}}{w_{\text{f}}}r_1 - r_3 - r_6 - r_9 \qquad (10)$$

$$\frac{dy_{GR}}{dt} = b\frac{w_{GR}}{w_f}r_2 - r_4 - r_7 \qquad (11)$$

$$\frac{dy_s}{dt} = r_3 + \frac{n_C^{GR} w_C}{w_{GR}} r_4 - r_8 + r_9 \qquad (12)$$

$$\frac{dN}{dt} = \rho\frac{N_A}{w_{PR}}r_3 - r_5, \qquad (13)$$

where y_{PR}, y_{GR}, and y_s are the mass fractions of precursors, growth species and soot, respectively, N the soot particle number density, ρ the mixture mass density, w_f, w_{PR}, w_{GR} and w_C the molar weights of fuel, PR, GR, and a carbon atom, respectively, n_C^{GR} the number of carbon atoms in GR, and N_A the Avogadro's number. The terms r_i, i = 1,...,9, appearing in Eqs (10)-(13) represent the corresponding rates of the processes (1)-(9). Specifically, the rates of the processes (1)-(3) were assumed to be in the form of global Arrhenius expressions:

$$r_1 = A_1 \exp(-E_1/RT) y_f, \qquad (14)$$

$$r_2 = A_2 \exp(-E_2/RT) y_f, \qquad (15)$$

$$r_3 = A_3 \exp(-E_3/RT) y_{PR}, \qquad (16)$$

where A_i and E_i are the preexponential factor and activation energy, respectively, of the ith process, R the universal gas constant, and T the temperature.

The rate of soot surface growth, r_4, was adopted following Leung et al. [20],

$$r_4 = A_4 \exp(-E_4/RT) S^{1/2} y_{GR}, \qquad (17)$$

where S is the soot total surface area. Leung and co-workers suggested that the growth rate being proportional to $S^{1/2}$ provides a better description of soot growth in laminar diffusion flames as compared to the traditional expression proportional to S. It should be emphasized, however, that this functional form has a completely empirical nature and accounts for only partial availability of the total soot surface area to the growth reactions as well as the overestimation of the total surface area caused by the assumption of monodisperse particle size distribution.

The rate of soot particle coagulation, r_5, is given by

$$r_5 = \frac{1}{2}\beta N^2. \qquad (18)$$

The collision frequency β is normally assumed to be in the free-molecular regime in most semi-empirical and detailed models [6-12, 20-23]. This assumption is usually valid for subatmospheric and atmospheric systems typically used for model validations. At high-pressure Diesel engine conditions, the gas mean free path becomes comparable with the particle size and soot coagulation cannot be treated as free-molecular process. Therefore, in the present work the coagulation constant was described with the expression suggested by Pratsinis [39] that covers the entire range of particle sizes,

$$\beta = \frac{\beta_{fm}\beta_{nc}}{\beta_{fm} + \beta_{nc}}.$$

The free-molecular collision frequency for the equal-sized particles, β_{fm}, is given by

$$\beta_{\mathrm{fm}} = 4\alpha\sqrt{\frac{6k_{\mathrm{B}}Td_{\mathrm{p}}}{\rho_{\mathrm{s}}}},$$

where α is the van der Waals enhancement factor, assumed equal 2 [40], k_B the Boltzmann constant, ρ_s the density of soot particle material assumed equal 2 g/cm^3, and

$$d_{\mathrm{p}} = \left(\frac{6y_s\rho}{\pi N\rho_s}\right)^{1/3}$$

the diameter of soot particle. The near-continuum coagulation constant, β_{nc}, is defined as

$$\beta_{\mathrm{nc}} = \frac{8k_BT}{\mu}\left(1+1.257\mathrm{Kn}\right), \qquad (19)$$

where μ is the molecular viscosity of the gas, Kn = $2\ell/d_p$ the Knudsen number, and ℓ is the gas mean free path. The factor of 1.257 appearing in Eq. (19) represents the near-continuum slip correction factor [39].

The rates of the processes (1)-(5), related to the fuel decomposition and soot formation, are assumed to be unaffected by turbulent mixing. For the oxidation rates (6)-(8), mixing is expected to play an important role. Thus, to accommodate mixing effects, as well as for consistency with the characteristic-time combustion model [37], the oxidation rates are written in the following form:

$$r_i = \frac{r_i^{\mathrm{kin}}r_i^{\mathrm{mix}}}{r_i^{\mathrm{kin}}+r_i^{\mathrm{mix}}},\ i=6,\ldots 8, \qquad (20)$$

where r_i^{kin} and r_i^{mix} are the kinetic and mixing oxidation rates, respectively. The functional form (20), i.e., harmonic mean of r_i^{kin} and r_i^{mix}, follows the approach of the characteristic-time combustion model used in the present study and represents the net steady-state result of two sequential processes, mixing and chemical reaction. In Eq. (20), the mixing rate is defined following the Magnussen's eddy-dissipation model [42]

$$r_i^{\mathrm{mix}} = c_i\frac{\varepsilon}{k}y,$$

where k is the turbulent kinetic energy, ε the rate of its dissipation, and y the mass fraction of oxidized species, i.e., y_{PR} for i=6, y_{GR} for i=7, and y_s for i=8. For the gas-phase processes, (6) and (7), the value of constant c_i was taken to be the same as for the other species in the characteristic-time combustion model, i.e., 10 [26]. In the case of soot oxidation, the constant c_8 is used as an adjustable parameter.

The kinetic parts of the gas-phase processes (6) and (7) are described with the global Arrhenius expressions,

$$r_6^{\mathrm{kin}} = A_6\exp\left(-E_6/RT\right)y_{\mathrm{PR}}\frac{\rho y_{\mathrm{O_2}}}{w_{\mathrm{O_2}}}, \qquad (21)$$

$$r_7^{\mathrm{kin}} = A_7\exp\left(-E_7/RT\right)y_{\mathrm{GR}}\frac{\rho y_{\mathrm{O_2}}}{w_{\mathrm{O_2}}}, \qquad (22)$$

where y_{O2} and w_{O2} are the mass fraction and the molecular weight of O_2, respectively. For the kinetic rate of soot surface oxidation, the widely-used expression of Nagle and Strickland-Constable [41] was utilized.

The rate of the process (9) is assumed to proceed with gas-kinetic collision rate,

$$r_9 = \sqrt{\frac{RT}{2\pi w_{PR}}} S y_{PR} \,. \qquad (23)$$

The Arrhenius parameters for the rate equations (14)-(17) and (21)-(22) are given in Table 1.

Table 1: Model kinetic parameters

Process	Rate parameters $k = A \exp(-E/RT)$	
	A (mol, cm, K, s)	E (kcal/mol)
1[a]	$9.35\ 10^{10}$	120.0
2[a]	$3.93\ 10^{8}$	49.0
3	$1.00\ 10^{10}$	50.0
4	$4.20\ 10^{4}$	12.0
6	$1.00\ 10^{12}$	40.0
7	$6.00\ 10^{13}$	50.0

[a] A was adjusted to achieve better agreement with the experimental results.

The actual implementation of the model requires the specific assignment of composition and thermochemical properties to the generic species GR and PR in order to account for conservation of mass and energy in the system. The composition and thermochemistry of the growth species GR were assumed to be those of acetylene, C_2H_2, which is commonly accepted as a key soot growth species in combustion systems. The physical "prototype" of the precursor species, PR, is a large polyaromatic molecule with relatively low H/C ratio. Therefore, PR is assumed to be composed only of carbon atoms, and its thermochemical properties were taken to be those of graphite on per carbon basis. The number of carbon atoms in PR was taken to be 50, which results in approximately a 1 nm size of the incipient soot particle. Similar to the precursor species, the thermochemical properties of soot particle material were assumed to be the same as those of graphite on a per carbon basis.

The rate equations (10)-(13) were incorporated in the KIVA-II code and coupled with the existing combustion model to account for the mass balance of main species (fuel, O_2, CO, and H_2) whose concentrations are being affected by the soot model. The system of coupled equations was solved with the implicit Euler method. It should also be pointed out that the rate equations (12)-(13) encounter a numerical problem when describing the burnout of soot particles. As can be seen, the oxidation of soot affects only the size of particles, while the particle number density remains the same. This assumption is reasonable if only moderate soot oxidation occurs. In an engine, one can expect situations where soot particles are being completely burned, so assuming the number density is unaffected leads to unrealistic particle sizes. Particle sizes that are substantially smaller than the size of the incipient particle or even a carbon atom can be predicted. In order to avoid this problem, it has been assumed that, if the rate of soot oxidation dominates over the inception and growth terms in Eq. (12) and the particle size decreases to the size of the incipient particle, further soot oxidation proceeds without change in particle size. Instead, the particle number density starts to decrease accounting for the soot mass loss.

Once implemented, the predictions of the cylinder pressure and heat release rate were indistinguishable for simulations with and without the soot model. That is continuity exists in the coupling of soot and combustion models through the mass and energy balances. Also, engine out emissions have been predicted and compared with experiments [47].

Experimental Results

The experimental measurements used for model validation were obtained by Tree and Foster [43,44] in a single-cylinder Cummins NH series direct-injection Diesel engine. The relevant engine specifications are presented in Table 2.

Table 2: Engine specifications

Bore	13.97 cm
Stroke	15.24 cm
Connecting Rod Length	30.48 cm
Displacement	2340 cm^3
Compression Ratio	15.5
Engine Speed	1300 rpm
Injector Type	Cummins PT
Number of orifices	8
Orifice Diameter	0.2 mm
Spray Angle	72°

The injection starts at approximately –22.5° ATDC and lasts approximately 33°. The injection profile needed for the KIVA calculations was estimated from the link load data as described by Gonzalez [45].

In-cylinder soot data were obtained using two optical diagnostics techniques based on the measurements of laser scattering and extinction, and radiation and extinction of light emitted by soot particles. The optical setup and the methods of data reduction are provided in detail elsewhere [43,44] and only briefly outlined below. The optical probe was mounted in the exhaust valve approximately 5 degrees counterclockwise from one of the fuel spray axes and about 4.8 cm from the center of the combustion chamber. The optical setup is shown schematically in Fig. 2. During the light scattering and extinction measurements (Fig. 2, top), the laser beam sent to the combustion chamber travels distance AB first and enters the scattering volume bounded by points B and C. For any element of the scattering volume ΔV, the light travels further the distance BD_1, where D_1 is location of the volume element, then gets scattered back to the cylinder head traveling the distance D_1E before reaching the receiving optical setup. The measured signal represents the summation of individual contributions from the volume elements along BC. Assuming the uniform soot distribution within the scattering measurement volume confined by the dotted lines, line BC and the cylinder head as shown in Fig. 2, the scattering signal is given by [43,44]

$$I_{\mathrm{sct}}(\lambda, f_{\mathrm{v}}, d_{\mathrm{p}}) = \alpha_{\mathrm{s}}(\lambda)\exp\Big[-k_{\mathrm{ext}}(\lambda, f_{\mathrm{v}}, d_{\mathrm{p}})$$

$$(L_{AB} + L_{BB'})\Big]\frac{Q_{\mathrm{sca}}(\lambda, f_{\mathrm{v}}, d_{\mathrm{p}})}{k_{\mathrm{ext}}(\lambda, f_{\mathrm{v}}, d_{\mathrm{p}})(1+\cos\gamma)}\Big[1-\exp\big(-k_{\mathrm{ext}}(\lambda, f_{\mathrm{v}}, d_{\mathrm{p}})L_{\mathrm{BC}}(1+\cos\gamma)\big)\Big], \qquad (25)$$

where α_s is a calibration constant, λ the wavelength of light, k_{ext} and Q_{sca} the extinction coefficient and volumetric scattering cross-section, respectively, determined from the Mie theory [46], L_{AB}, $L_{BB'}$, and L_{BC} the lengths of AB, BB' and BC, respectively, and γ the angle ABB'. The experimental data taken at two different wavelengths (488 and 514.5 nm) provided the system of two equations obtained by substitution of values of λ into Eq. (25) that was solved numerically with respect to f_v and d_p. Particle number density is derived from the geometric relationship, $N = 6f_{\mathrm{v}}/\pi d_{\mathrm{p}}^3$.

In the case of radiation and extinction measurements, the flame radiation at two different wavelengths (514.5 and 850 nm) was measured. Each individual volume element ΔV located at point D_2 within the radiation measurement volume bounded by the dotted lines, the cylinder head and the piston outline (Fig. 2, bottom) emits light that subsequently travels the distance D_2E before entering the receiving optical setup. Again, assuming the uniform distributions of temperature and soot fields within the radiation measurement volume and neglecting the contributions of the radiation sources other than soot particles, the radiation signal can be written as [43,44]:

$$I_{\mathrm{rad}}(\lambda, f_{\mathrm{v}}, d_{\mathrm{p}}) = \alpha_{\mathrm{r}}(\lambda)\left[1 - \exp\left(-k_{\mathrm{ext}}(\lambda, f_{\mathrm{v}}, d_{\mathrm{p}})L_{\mathrm{PH}}\right)\right] P(\lambda, T) \quad (26)$$

where α_r is a calibration constant and $P(\lambda, T)$ is the Plank's function. The parameter L_{PH} represents the effective length of the radiating volume that was estimated to be 0.6 of the distance between the cylinder head and the piston bowl at the particular moment of the engine cycle [43,44]. Radiation measurements at two wavelengths combined with one set of scattering data at λ = 514.5 nm provide the system of three equations that was solved for f_v d_p, and T. The optical signals used to obtain the solutions for soot properties were statistically averaged over about 200 engine cycles.

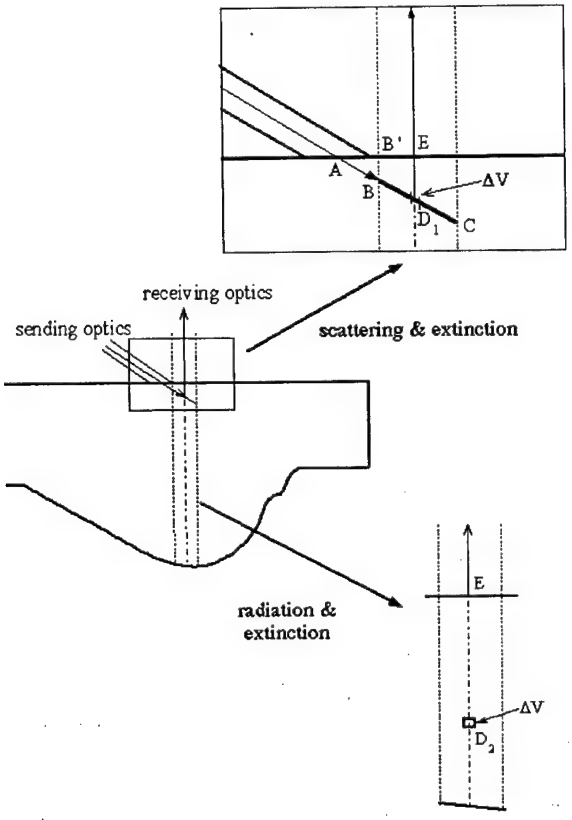

Figure 2: A schematic cross-section of the optical probe and expanded views of scattering and radiation measurement volumes [42,43].

The computational mesh used in the present study is presented in Fig. 3. It represents one-eighth of the engine combustion chamber (i.e., a 45° sector) for computational efficiency since the injector has eight holes. There were 28 cells in the radial direction, 20 cells in the azimuthal direction and 28 cells in the axial direction.

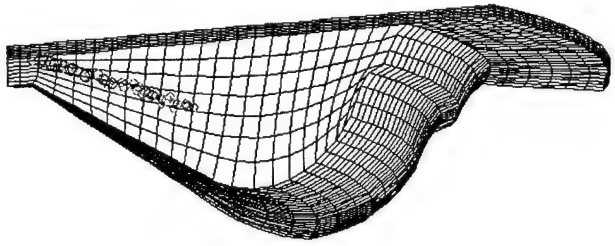

Figure 3: Perspective view of the computational grid and fuel droplet distribution at top dead center.

RESULTS AND DISCUSSION

As a first step of the simulation, the calibration of ignition, combustion, and spray atomization submodels was performed in order to reproduce the in-cylinder pressure and the rate of heat release observed experimentally. The result of this

calibration is presented in Figure 4. As can be seen, the agreement between the experimental measurements and the model results are very good. The shape of the heat release curve exhibiting no significant premix burn typical of the Cummins PT injection system is reproduced very well (Fig.4, bottom panel).

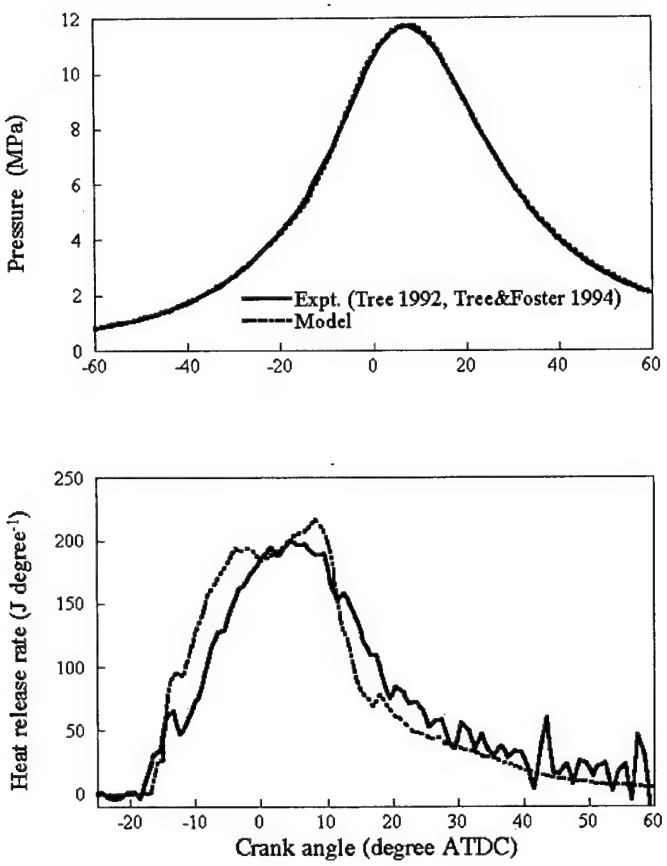

Figure 4: Measured and predicted in-cylinder pressure (top) and the rate of heat release (bottom).

Next, the soot model was calibrated against the experimental data of Tree and Foster [43, 44]. Preliminary sensitivity runs [47] indicated that the most sensitive parameters affecting predictions of soot mass are the rate of formation of growth species, r_2, and soot oxidation rate, r_8. To obtain a reasonable agreement with the experimental data, the preexponential factor of reaction (2) and constant c_8 were adjusted. In addition, since the rate of PR formation strongly influences predictions of particle number density the preexponential factor of reaction (1) was adjusted as well. The adjusted preexponential factors are given in Table 1, and the value of c_8 was 10. As explained in the previous section, the actual experimental measurements and their reduction were rather complex and based on a number of assumptions. In particular, uniform spatial soot distribution within the measurement volumes was assumed. Considering the uncertainties in the experimental data reduction and the simplifications accepted in the model, it is reasonable to adopt some simple but yet consistent criterion for comparison of model predictions and the experimental measurements. Thus, the soot concentration in the most sooting computational cell located within the scattering measurement volume was used as a reference for comparison with the experimental data. The results of this comparison are presented in Figure 5. Although the timing of soot appearance is somewhat overpredicted by the model, the agreement for soot volume fraction appears to be reasonably good in terms of the absolute magnitude and the overall shape of the curve. The agreement for the particle number density and particle size is worse, but still reasonable considering the fact that the optical methods are normally biased towards larger particles, which tends to overestimate the particle size and underestimate the number density. It should be pointed out that the search for better agreement via better model calibration or adjustment of the probe location within the reasonable range was not pursued due to the proximity of this comparison discussed above. As can be seen from the contour plots illustrating the migration of soot particle cloud, also shown in Fig. 5, the observed temporal maximum in soot volume fraction is mainly caused by the motion of soot particles in and out of the optical probe, as was hypothesized by Tree and Foster [43, 44]

To gain the understanding of the model predictions in terms of the conceptual picture of soot formation and oxidation in an engine, a more detailed analysis of the computational results has been performed.

According to the model, the autoignition occurs near the initial portion of the spray at about –16.5 degrees ATDC (Fig. 6, c). Analysis of the conditions prior to the ignition indicates that the ignition takes place close to the center of a vortex formed between the fuel spray and the cylinder head (Fig. 6, a,b). The promoting effect of the vortex on the autoignition can be viewed in several ways. First of all, the vortex improves mixing and, therefore, helps in preparation of ignitable mixture. In addition, by supplying the fresh air heated during compression, it prevents the decrease in the mixture temperature caused by intensive fuel vaporization. Finally, one can also speculate that the center of the vortex is a good candidate for the ignition location since, due to low strain rate, the radical pool there would keep accumulating and would not be destroyed by transport processes.

Additional zero-dimensional calculations performed in the course of the present study indicated that the Shell autoignition model, as implemented in the ERC version of KIVA-II, predicts that moderately rich homogenous mixture would have a shorter ignition delay at typical engine conditions as compared to stoichiometric and lean mixtures. This result is consistent with the recent observations of high-pressure n-heptane ignition in a shock tube [48, 49]. Yet, the equivalence ratio of the igniting computational cell was about 0.2 in the present engine simulations, i.e., the ignition took place at extremely fuel-lean conditions. This seemingly controversial result is explained by the fact that, according to the present model, the autoignition conditions are mainly determined by processes of local mass and heat transfer rather than homogenous chemical kinetics. The conclusion regarding the decisive influence of transport processes on the autoignition has been also reached by Wan et al. [16] based on the KIVA calculations with detailed chemical kinetics incorporated using the flamelet approach. This result contradicts the suggestion of Dec [50] that combustion in a similar engine initially occurs exclusively at fuel-rich conditions.

However, it is not clear whether this disagreement is caused by the misrepresentation of the actual ignition process by the simplified Shell kinetics [34] used in the present model or the differences in the experimental conditions of Tree and Foster [43,44] and Dec [50] who used a different injection system, Cummins CELECT.

Furthermore, the comparison to Dec's work could be misleading since his autoignition event is not well defined. Dec notes observing the first chemiluminescence upstream of the liquid jet before the formation of rich mixture on the tip of the liquid jet. The simulation would classify such an occurrence as autoignition. Hence, the model predictions may not be contradictory to the experimental results.

Further development of the spray flame and initial soot formation is presented in Fig. 7. As can be seen, the spray flame appears to be essentially transient in its nature. Upon ignition, the flame propagates along the spray periphery, reaches the tip of the liquid spray and forms a three-dimensional structure that looks like a wine glass with a long stem, with the highest temperatures observed around the "neck" that connects the "stem" with the "cup". Inside the "stem" formed by a diffusion flame around the spray periphery, intensive droplet evaporation and formation of fuel-rich mixture takes place. Then, this mixture passes through the high-temperature "neck" and enters inside the flame "cup". Intensive soot formation started inside the observed "stem" continues in the "cup" supported by a heat flux from the "cup" walls. As the process develops even further and the flame propagates closer to the piston bowl, the "cup" walls expand and finally connect together surrounding the soot-forming contents of the "cup" and reinitiating soot growth at the leading edge of soot cloud.

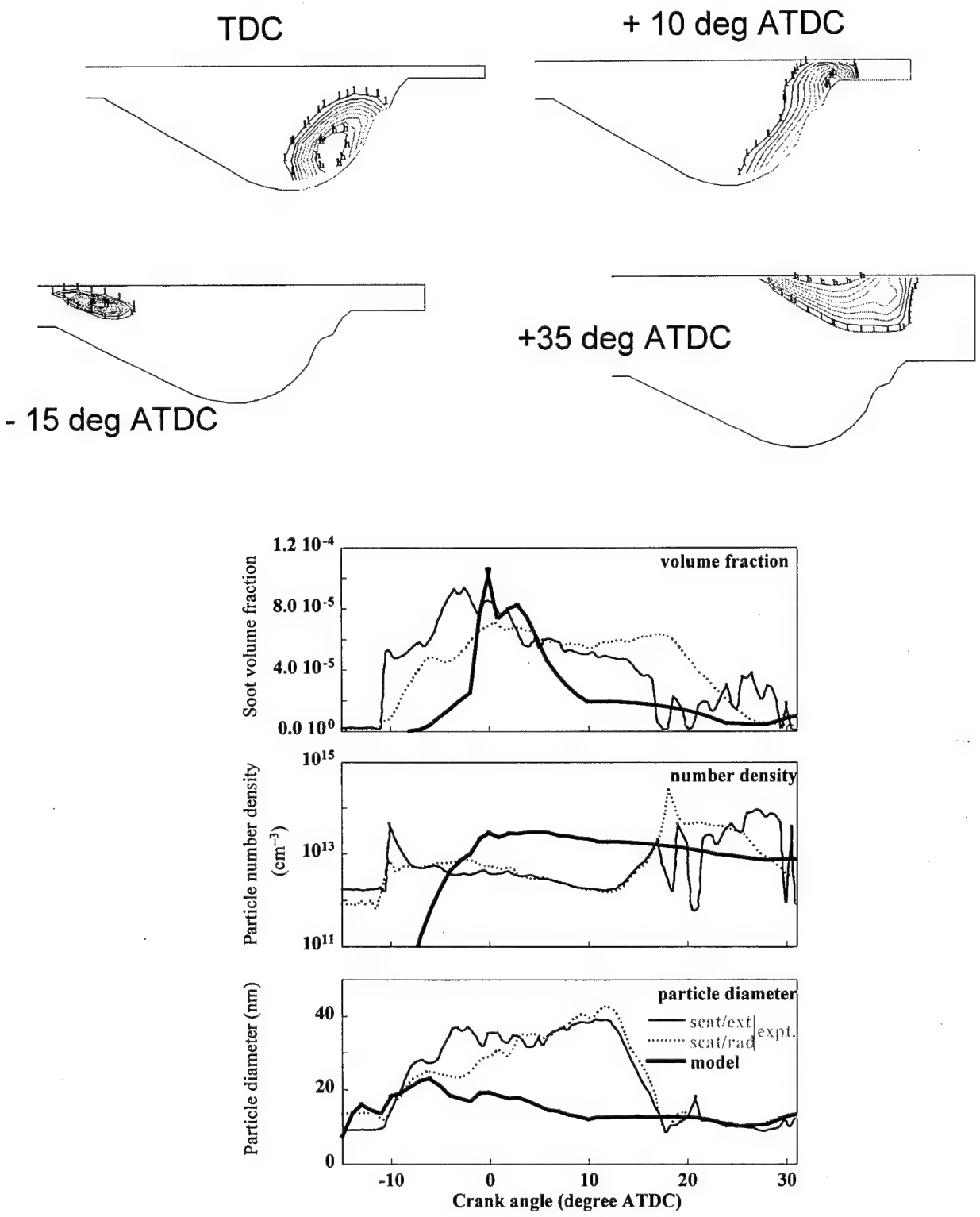

Figure 5: Comparison of measured and predicted soot particle properties. The sequence of contour plots on the top illustrates the movement of soot particle cloud.

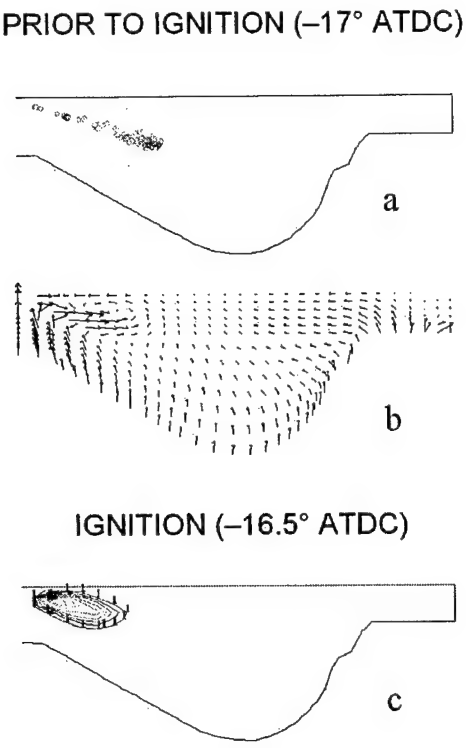

Figure 6: Contour plots showing the conditions before (a-b) and after (c) autoignition. (a) spray distribution; (b) flow velocity, and (c) temperature.

We note that the model does not predict the existence of a rich premixed flame on the tip of the liquid spray as suggested by Dec [50]. It predicts that fuel-lean and near-stoichiometric regions always dominate the heat release in the system. Nevertheless, the images shown in Fig. 7 reveal a qualitative similarity with the experimental observations [50]. In particular, the initial location of the soot cloud and its temporal evolution are very similar to the schematic pictures derived from laser-sheet image analysis [50]. The principal difference between the present computational results and the interpretation of the experimental observations reported by Dec is the existence of the diffusion flame around the spray periphery ("stem-cup" structure) predicted by the model. In Ref. 50, it was suggested that the diffusion flame develops at a later stage of the process following the period of rich nearly premixed combustion.

Further development of soot cloud can be seen from the contour plots on the top of in Fig. 5. After the bowl wall impingement, the soot cloud follows the flow around the cylinder outline while undergoing a continuous oxidation. The final soot "survival" occurs in the low-temperature regions close to the cylinder head. To illustrate the overall history of soot formation and destruction during the engine cycle, a cumulative soot mass probability density function with respect to the temperature and the equivalence ratio, ϕ, was derived in a fashion explained below. The detailed computational outputs at each crank angle were analyzed and non-normalized soot mass distributions in the cylinder with respect to the temperature and the equivalence ratio were obtained. Then, the individual distributions were summed and the cumulative mass-time distribution was obtained. The result of this procedure is presented in Fig. 8. As can be seen, the soot occurrence is localized within a rather complex-shaped region. The region is divided in two parts connected with a relatively narrow "corridor". The first part represents a distorted triangle confined between the temperatures of about 1500-3000 K and the equivalence ratios of 0.6 to 7. Most of soot formation appears to be in a relatively narrow region of the triangle, at the temperatures of about 2100-2400 K and equivalence ratios of 1.5 to 2. The boundaries of the triangle can be interpreted as follows. The bottom boundary is an "oxidation" limit, i.e., below this line, the equivalence ratio is so low that soot gets completely oxidized. Outside the left boundary, the soot formation is thermally-limited, i.e., the rates of soot formation are not fast enough to produce significant amounts of soot even at high equivalence ratios. Finally, the right boundary of the triangle is a thermodynamic limit which mainly reflects the dependence of adiabatic flame temperature upon the equivalence ratio. In other words, although high-equivalence-ratio and high-temperature conditions outside this boundary represent a perfect environment for soot formation and growth, such conditions simply are not encountered during the engine cycle. The top corner of the triangle is a region where soot survives oxidation by entering

fuel-rich regions, however, this survival is only temporary since these regions will eventually be destroyed by mixing. The ultimate soot survival takes place in the second part of soot occurrence region located in the bottom left corner of Fig. 8. Equivalence ratios in this region are extremely small, however, the temperatures are so low that soot oxidation becomes insignificant. Physically, such conditions are realized in the vicinity of the cylinder walls at the end of the cycle.

SUMMARY AND CONCLUSIONS

Phenomenological model of soot formation and oxidation presented in the present work was shown to predict reasonably well the in-cylinder soot concentration, particle number density, and particle size measured experimentally in a Cummins NH-series heavy-duty Diesel engine. In addition, the qualitative conceptual picture of soot formation derived from the present computational results appear to be consistent with in-cylinder laser-sheet image analysis reported for a similar engine [50]. The computational model does not predict the existence of a rich premixed flame being responsible for the initial heat release and soot formation as suggested by Dec [50]. Instead, the results indicate a transient development of the diffusion flame structure around the spray periphery and close to spray tip, which leads to the spatial and temporal history of soot particle cloud consistent with the actual experimental observations. Analysis of the model predictions shows that the majority of soot mass during the cycle is formed under relatively narrow range of conditions, i. e., at about 2200-2400 K and the equivalence ratios of 1.5-2. The ultimate survival of soot at the end of the cycle occurs close to the cylinder head at extremely fuel-lean conditions with below 0.5 and low temperatures around 1000 K, which prohibits further oxidation.

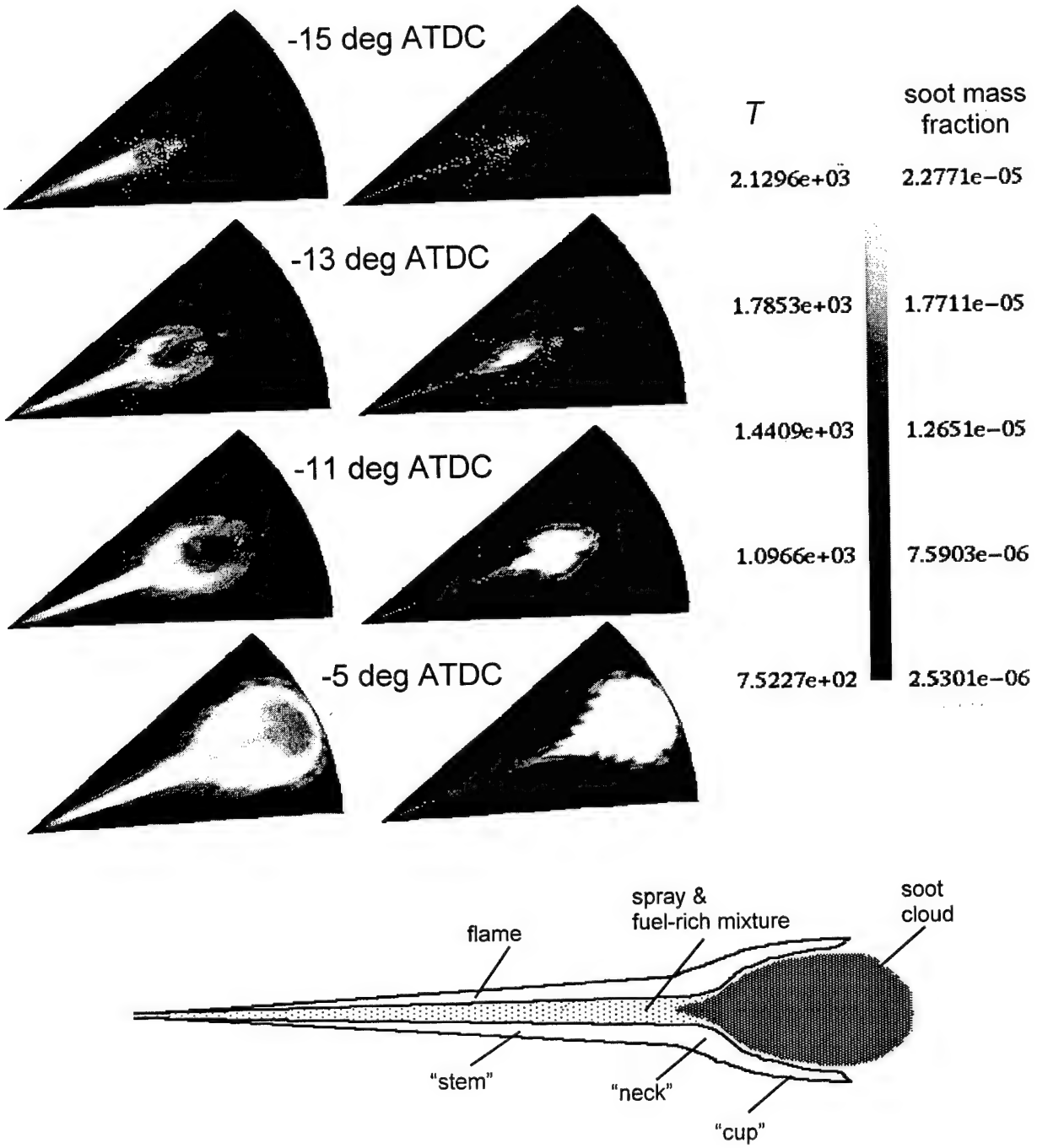

Figure 7: Temporal sequence of development of the temperature and soot fields in the plane of fuel jet. White dots represent the droplets of liquid fuel.

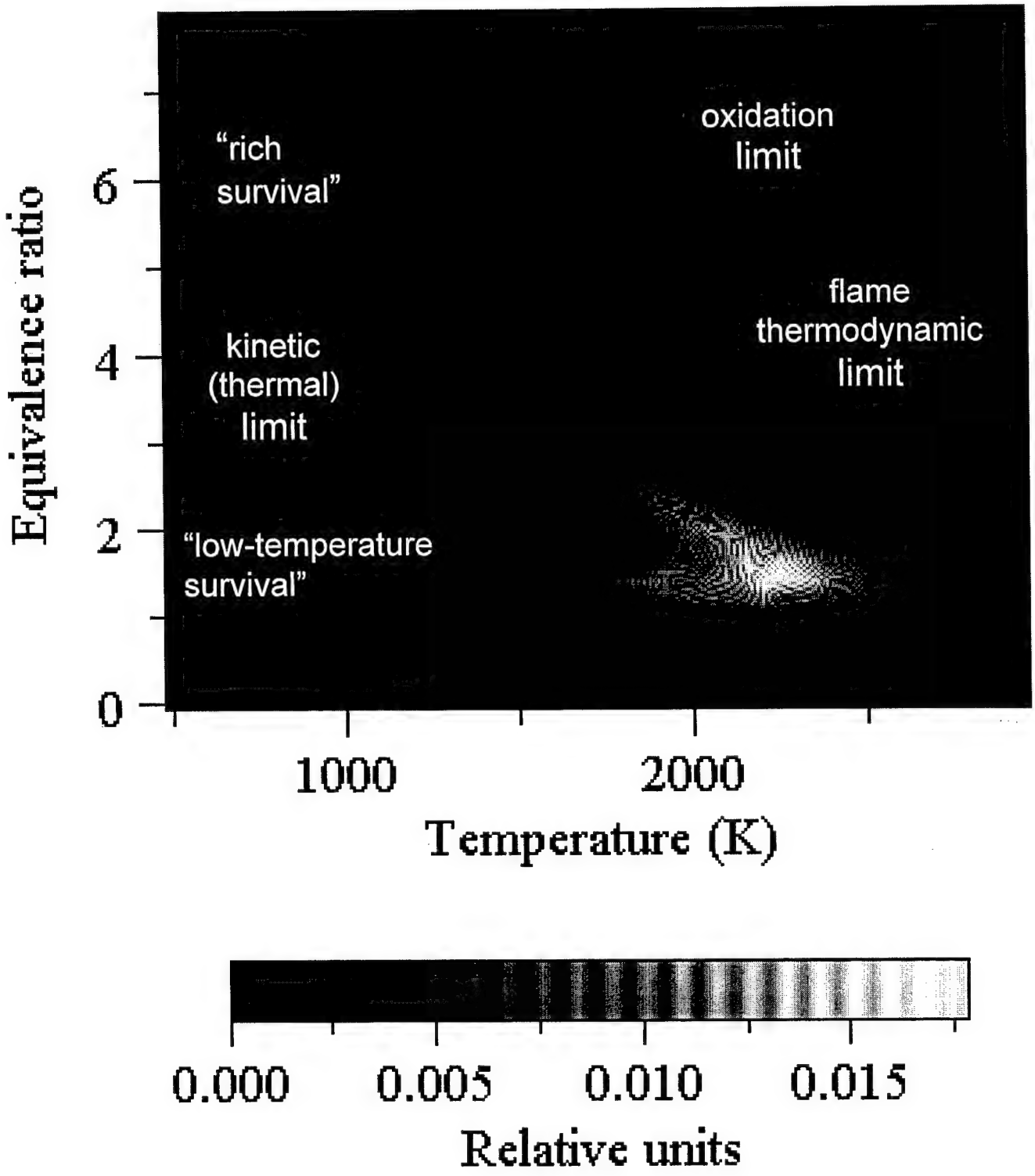

Figure 8: The cumulative history of soot formation and destruction during the engine cycle (see text).

References

1. Browner M. C., "Smog and Soot: Updating Air Quality Standards", *Public Health Reports*, **112**, 366-367, 1997.
2. Hentschel, W., "Modern Tools for Diesel Engine Combustion Investigation", Twenty-Sixth Symposium (International) on Combustion, The Combustion Institute, Pittsburgh, p. 2503-2515, 1996.
3. Bockhorn, H., Ed., *Soot Formation in Combustion: Mechanisms and Models*, Springer-Verlag, Heidelberg, 1994.
4. Kennedy, I. M., "Models of Soot Formation and Oxidation", *Prog. Energy Combust. Sci.*, **23**, 95-132, 1997.
5. Khan, I. M. and Greeves, G., "A Method for Calculating the Formation and Combustion of Soot in Diesel Engines", *Heat Transfer in Flames*, Afgan, N. H and Beer, J. M., Eds., Scripta, Washington, DC, 1974.
6. Yoshihara, Y., Kazakov, A., Wang, H., and Frenklach, M. "Reduced Model of Soot Formation: Application to the Natural Gas-Fueled Diesel Combustion", Twenty-Fifth Symposium (International) on Combustion, The Combustion Institute, Pittsburgh, pp. 9412-948, 1994.
7. Pitsch, H., Wan, Y. P., and Peters, N. "Numerical Investigation of Soot Formation and Oxidation under Diesel Engine Conditions", SAE Technical Paper 952357.
8. Pitsch, H., Barths, H., and Peters, N. "Three-Dimensional Modeling of NO_x and Soot Formation in DI-Diesel Engines Using Detailed Chemistry Based on the Interactive Flamelet Approach", SAE Technical Paper 962057.
9. Astill, A. G., Smith, A. P., and Stopford, P. J., "Soot Formation and Oxidation: Development of a Numerical Model and Comparison with Experimental Data from a High Pressure Diesel Combustion Bomb", SAE Technical Paper 97P-321.
10. Frenklach, M. and Wang. H., "Detailed Modeling of Soot Particle Nucleation and Growth", The Twenty-Third Symposium (International) on Combustion, The Combustion Institute, Pittsburgh, pp. 1559-1566, 1990.
11. Kazakov, A., Wang, H., and Frenklach, M., "Detailed Modeling of Soot Formation in Laminar Premixed Flames at a Pressure of 10 Bar", *Combust. Flame*, **100**, 111-120 (1995).
12. Mauss, F., Schäfer, T., and Bockhorn, H., "Inception and Growth of Soot Particles in Dependence on the Surrounding Gas-Phase", *Combust. Flame*, **99**, 697-705 (1994).
13. Marquardt, M., Mauss, F., Jungfleisch, B., Suntz, R., and Bockhorn, H., Twenty-Sixth Symposium (International) on Combustion, The Combustion Institute, Pittsburgh, pp. 2343-2350, 1996.
14. Marinov N. M., Pitz, W. J., Westbrook, C. K., Castaldi, M. J., Senkan, S. M., "Modeling of Aromatic and Polycyclic Aromatic Hydrocarbon Formation in Premixed Methane and Ethane Flames", *Combust. Sci. Technol.*, **116**, 211-287, 1996.
15. Wang H., Frenklach M., "Detailed Kinetic Modeling Study of Aromatics Formation in Laminar Premixed Acetylene and Ethylene Flames", *Combust. Flame*, **110**, 173-221, 1997.
16. Wan, Y. P., Pitsch, H., and Peters, N. "Simulation of Autoignition Delay and Location of Fuel Sprays Under Diesel-Engine Relevant Conditions", SAE Technical Paper 971590.
17. Reitz, R. D., "Modeling Atomization Process in High-Pressure Vaporizing Sprays", *Atomization Spray Technol.*, **3**, 309-337, 1987.
18. Ricart, L. M., Xin, J., Bower, G. R. and Reitz, R. D., "In-Cylinder Measurement and Modeling of Liquid Fuel Spray Penetration in a Heavy-Duty Diesel Engine", SAE Technical Paper 971591.
19. Tesner, P. A., Snegiriova, T. D., and Knorre, V. G., "Kinetics of Dispersed Carbon Formation", *Combust. Flame*, **17**, 253-260, 1971.
20. Leung, K. M., Lindstedt, R. P., and Jones, W. P., "A Simplified Reaction Mechanism of Soot Formation in Nonpremixed Flames", *Combust. Flame*, **87**, 289-305, 1991.
21. Fairweather, M., Jones, W. P., Ledin, H. S., Lindstedt, R. P., "Predictions of Soot Formation in Turbulent, Non-Premixed Propane Flames", The Twenty-Fourth Symposium (International) on Combustion, The Combustion Institute, Pittsburgh, pp. 1067-1074, 1992.
22. Kennedy, I., Kollmann, W., and Chen, J.-Y., "A Model for Soot Formation in a Laminar Diffusion Flame", *Combust. Flame*, **81**, 73-85, 1990.
23. Moss, J. B., Stewart, C. D., and Syed, K. J., "Flowfield Modeling of Soot Formation at Elevated Pressure", The Twenty-Second Symposium (International) on Combustion, The Combustion Institute, Pittsburgh, pp. 413-423, 1988.
24. Hiroyasu, H. and Kadota, T., "Models for Combustion and Formation of Nitric Oxide and Soot in DI Diesel Engines", SAE Technical Paper 760129.
25. Belardini, P., Bertoli, C., Ciajolo, A., D'Anna, A., and Del Giacomo, N., "Three-Dimensional Calculations with In-Cylinder Sampling Valve Data", SAE Technical Paper 922225.
26. Han, Z., Uludogan, A., Hampson, G. H. and Reitz, R. D., "Mechanism of Soot and NO_x Emission Reduction Using Multiple-Injection in a Diesel Engine", SAE Technical Paper 960633.
27. Belardini, P., Bertoli, C., Del Giacomo, N., and Iorio, B., "Soot Formation and Oxidation in a DI Diesel Engine: A Comparison Between Measurements and Three Dimensional Computations", SAE Technical Paper 932658.

28. Belardini, P., Bertoli, C., Camaretti, M. C., and Del Giacomo, N., "A Coupled Diesel Combustion and Soot Formation Model for KIVA-II Code: Characteristics and Experimental Validation", The Third International Symposium on Diagnostics and Modeling of Combustion in Internal Combustion Engines, Yokohama, Japan, 1994, p. 315-323.
29. Belardini, P., Bertoli, C., Beatrice, C., D'Anna, A., and Del Giacomo, N., "Application of a Reduced Kinetic Model for Soot Formation and Burnout in Three-Dimensional Diesel Combustion Computations", Twenty-Sixth Symposium (International) on Combustion, The Combustion Institute, Pittsburgh, p. 2517-2524, 1996.
30. Fusco, A., Knox-Kelecy, A. L., and Foster, D. E., "Application of a Phenomenological Soot Model for Diesel Engine Combustion", The Third International Symposium on Diagnostics and Modeling of Combustion in Internal Combustion Engines, Yokohama, Japan, 1994, p. 571-576.
31. Amsden, A. A., O'Rourke, P. J., and Butler, T. D., "KIVA-II – A Computer Program for Chemically Reactive Flows with Sprays", Los Alamos National Labs, LA-11560-MS, 1989.
32. Reitz, R. D. and Rutland, C. J., "Developing and Testing of Diesel Engine CFD Models", *Prog. Energy Combust. Sci.*, **21**, 173-196, 1995.
33. Han, Z. and Reitz, R. D. "Turbulence Modeling of Internal Combustion Engines Using RNG k-ε Models", *Combust. Sci. Technol.*, **106**, 267-280, 1995.
34. Halstead, M. P., Kirsch, L. J., and Quinn, C. P., "The Autoignition of Hydrocarbon Fuels at High Temperatures and Pressures – Fitting of a Mathematical Model", *Combust. Flame*, **30**, 45-60, 1977.
35. Kong, S.-C. and Reitz, R. D., "Miltidimensional Modeling of Diesel Ignition and Combustion Using a Multistep Kinetic Model", *J. Engineering Gas Turbines Power*, **115**, 781-789, 1993.
36. Abraham, J., Bracco, F. V., and Reitz, R. D., "Comparisons of Computed and Measured Premixed Charge Engine Combustion", *Combust. Flame*, **51**, 141-143, 1983.
37. Kong, S.-C., Han, Z., and Reitz, R. D., "The Development and Application of a Diesel Ignition and Combustion Model for Multidimensional Engine Simulation", SAE Technical Paper 950278.
38. Kazakov, A. and Frenklach, M., "On the Relative Contribution of Acetylene and Aromatics to Soot Particle Surface Growth", *Combust. Flame*, **112**, 270-274, 1998, and the references therein.
39. Pratsinis, S. E., "Simultaneous Nucleation, Condensation and Coagulation in Aerosol Reactors", *J. Colloid Interface Sci.*, **124**, 416-427, 1987.
40. Harris, S. J., and Kennedy, I. M., "The Coagulation of Soot Particles with van der Waals Forces", *Combust. Sci. Technol.*, **59**, 443-454, 1988.
41. Nagle, J. and Strickland-Constable, R. F., "Oxidation of Carbon between 1000-2000° C", Proc. of the Fifth Carbon Conf., Pergamon, London, 1962, pp. 154-164.
42. Magnussen, B. F. and Hjertager, B. H., "On Mathematical Modeling of Turbulent Combustion with Special Emphasis on Soot Formation and Combustion", The Sixteenth Symposium (International) on Combustion, The Combustion Institute, Pittsburgh, pp. 719-729, 1977.
43. Tree, D. R., "Soot Particle Size and Number Density Measurements in a Direct Injection Diesel Engine Using Light Scattering, Radiation and Extinction", Ph. D. Thesis, University of Wisconsin-Madison, 1992.
44. Tree, D. R., and Foster, D. E. "Optical Soot Particle-Size and Number Density-Measurements in a Direct-Injection Diesel-Engine", *Combust. Sci. Technol.*, **95**, 313-331, 1994.
45. Gonzalez, D. M. A., "A Computational Study of In-Cylinder Cold Starting Processes in a Diesel Engine", M. Sc. Thesis, University of Wisconsin-Madison, 1990.
46. Bohren, C. F. and Huffman, D. R. *Absorption and Scattering of Light by Small Particles*, Wiley, New York, 1983.
47. Kazakov, A. and Foster, D. E., in preparation.
48. Ciezki and Adomeit, *Combustion and Flame*, vol 93, pp 421-433, 1993
49. Minetti, Carlier, Ribaucour, Therssen and Sochet, *Combustion and Flame*, Vol. 102, pp 298-309, 1995
50. Dec, J. E., "A Conceptual Model of DI Diesel Combustion Based on Laser-Sheet Imaging", SAE Technical Paper 970873, 1997.

DIESEL COMBUSTION MODELING

The goal of Project 3: Diesel Combustion Modeling was to develop and test a flamelet based combustion model for diesel engines. In flamelet combustion models, chemistry and kinetic effects are decoupled from turbulence effects. This can make modeling easier and permits the use of stronger theoretical foundations.

Overall, the project has been very successful. Physically motivated flamelet combustion models have been implemented and tested with a variety of engine data. The comparison with engine data is very good and the model provides additional detailed information that was not available in previous models. In addition,

the flamelet approach is configured to take advantage of new large eddy simulation (LES) turbulence models currently under development.

The work proceeded in two phases. In the first phase, a general procedure for adapting flamelet approaches for diesel engines was developed. The second phase of the project has focused on refining the flamelet model, primarily in terms of adding additional chemical kinetics effects.

Developing and implementing a flamelet combustion model for diesel engine applications required several innovative modeling strategies. This was due to the complex nature of diesel combustion which has three distinct phases: ignition, premixed combustion and diffusion combustion. The important physical processes in each phase were defined and modeled as directly as possible. Also, two transition steps were required to model the progression of combustion between each of the three phases.

The ignition or low temperature combustion phase was modeled using the multi-kinetic step Shell ignition model (Kong and Reitz, 1993). The transition to high temperature, premixed combustion was accomplished using criteria based on local temperatures and heat release rates. The high temperature premixed combustion was modeled using a global Arrhenius equation for the reaction rate. This was later improved in the second phase of the project.

The transition from premixed combustion to mixing limited diffusion combustion was based on a local critical Damkohler number. The Damkohler number relates flow mixing time to chemical reaction time and is the proper choice of transition to mixing controlled combustion. The diffusion combustion phase was modeled using a flamelet approach based on the coherent flamelet concepts (Marble and Broadwell, 1977, and Candel, et al., 1988). This approach uses the concept of flame sheets represented by a flame area per unit volume variable called Σ. The flame area is transported by fluid turbulence, is increased by fluid stretching and flame propagation, and is decreased by fuel depletion and extinction processes.

Several aspects of diesel combustion required extra attention in implementing the flamelet model. Since fuel vapor comes from evaporating spray drops, the sub-grid processes in a given computational cell can become fairly complex. The fuel evaporation can occur in either a premixed or diffusion burning cell. This required keeping track of premixed fuel vapor as separate from fuel vapor which is not premixed and will burn in a diffusion combustion mode. Another complexity is that the diffusion flame effectively separates the cell into an oxidizer side and a fuel side. The distribution of inerts on each side was found to have some effect on the results so an inerts transport was also added. This was later found to be less important than other processes that were improved in the second phase of the project.

The coherent flamelet modeling approach is able to reproduce the characteristic features of diesel engine combustion, including the ignition delay, the short, rapid premixed combustion phase, and the longer diffusion combustion phase (Musculus and Rutland, 1995). The sensitivity of the combustion events to several of the model parameters was examined and the results were used to pick the optimum settings for the model. The Σ production parameter and destruction parameter had similar effects on the location of the peak pressure. It was also found that the proper rate of strain for determining flame production by stretch lies somewhere between the large and small scale turbulent strains. The effects of the strain due to the mean flow strain were minimal.

Experiments on a Caterpillar model E 300, # 1Y0540 engine, a Tacom LABECO research engine, and a single cylinder version of a Cummins N14 production engine were used to validate the predictions of the initial phase of the model. For example, Figure 1 shows a comparison of the heat release from the model with the data from the Tacom engine. The agreement is reasonable for the first phase of the model. More importantly, the figure shows the additional detail concerning the type of combustion that is now captured by the model.

The model was also studied by examining the spatial resolution of the results inside the engine cylinder. The location and magnitude of modeled heat releases, flame areas, and equivalence ratios were found to be realistic although no data is available for direct comparison. For example, it was found that the diffusion burn heat release and flame area density were largest in an envelope around the spray (see Figure 2).

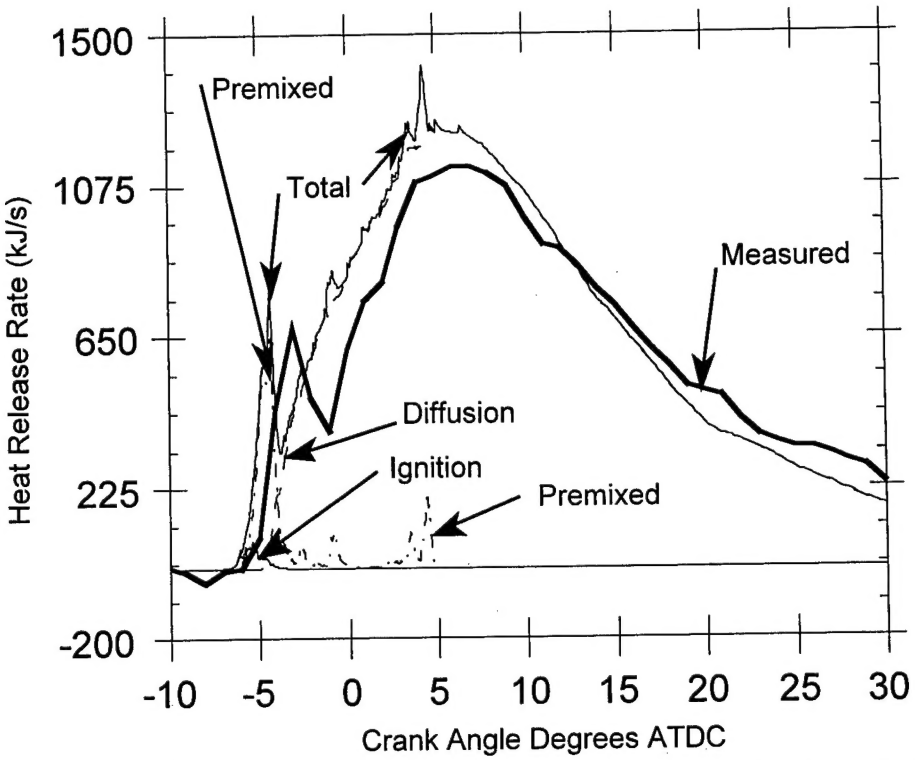

Figure 1: The ignition, high temperature kinetics (premixed), and diffusion burn components of the computational heat release and the measured heat release for the Tacom engine.

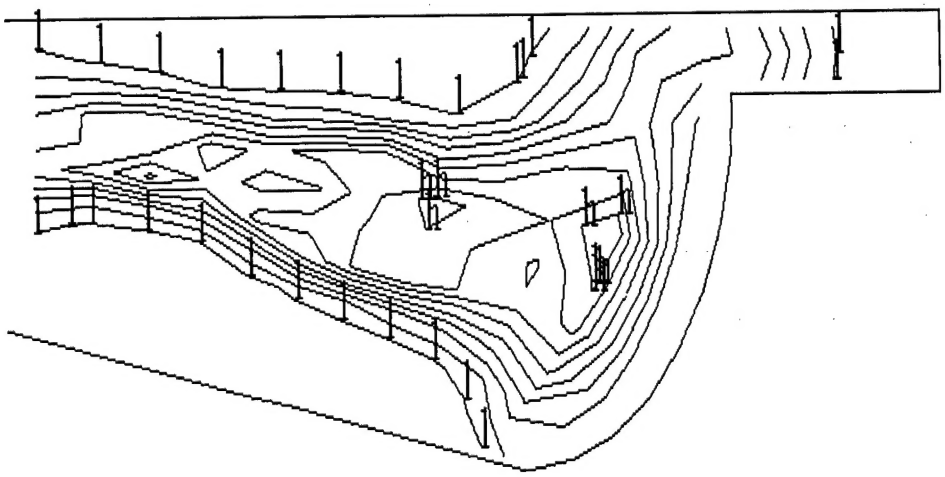

Figure 2: Contours of the diffusion flame heat release rate at a crank angle of +10 for the Tacom engine

In the second phase of the project, improvements to components of the model were undertaken. Initial plans called for including a flame curvature parameter that would provide an extra length scale for mixing. Preliminary analysis indicated that this would not be as useful as improvements to other parts of the model.

The first improvement was to isolate the premixed fuel to the oxidizer side of a computational cell in those cases in which both premixed fuel and non-premixed fuel exist at the same time. This was found to improve the transition from premixed to diffusion combustion by making the differences in heat release rates less severe.

The next improvement was to change the underlying fuel consumption kinetics from a single step reaction to a two step reaction based on the following chemical steps:

$$C_{14}H_{30} + 14.5O_2 \Rightarrow 14CO + 15H_2O \qquad (1)$$

$$CO + 0.5O_2 \Rightarrow CO_2 \qquad (2)$$

The first step is the primary fuel conversion and the second step is CO oxidation. These two steps are used in the premixed phase of combustion which is still based on a time scale rate term. Separation into these two steps turns out to be very important because of the very different kinetic time scales involved. The fuel density in equation (1) is the density of premixed fuel, which is determined by a transport equation. The transport equation contains source terms due to fuel-air mixing and combustion.

The third improvement involves the diffusion combustion phase. The reaction rate and mixing are still determined using the Σ equation. However, now this is used for reaction step (1) where CO and H_2O are the products. In the diffusion flame, the CO oxidation in reaction step (2) is modeled more like a partially stirred reacting and a mixing time scale. The Σ model for diffusion combustion is used when the Damköhler number is large and the kinetic rates for the fuel conversion are much faster than the mixing rates. Therefore the conversion of fuel to CO and H_2O.is assumed to be mixing limited. The kinetics of the CO oxidation are slower than the kinetics for the fuel conversion, therefore the CO oxidation is not assumed to be mixing limited.

Calculations using the improved coherent flamelet model were compared with data from the Sandia National Laboratories heavy duty diesel engine. This engine is based on a Cummins N14 with modifications for extensive optical access and instrumentation. The comparison between the measured and simulated cylinder pressure and heat release rates are shown in Figure 3. In general, there is very good agreement between the simulations and the flamelet model. The peak pressure magnitude and timing match very well. The premixed combustion spike and the main diffusion combustion phase are also captured very well by the model.

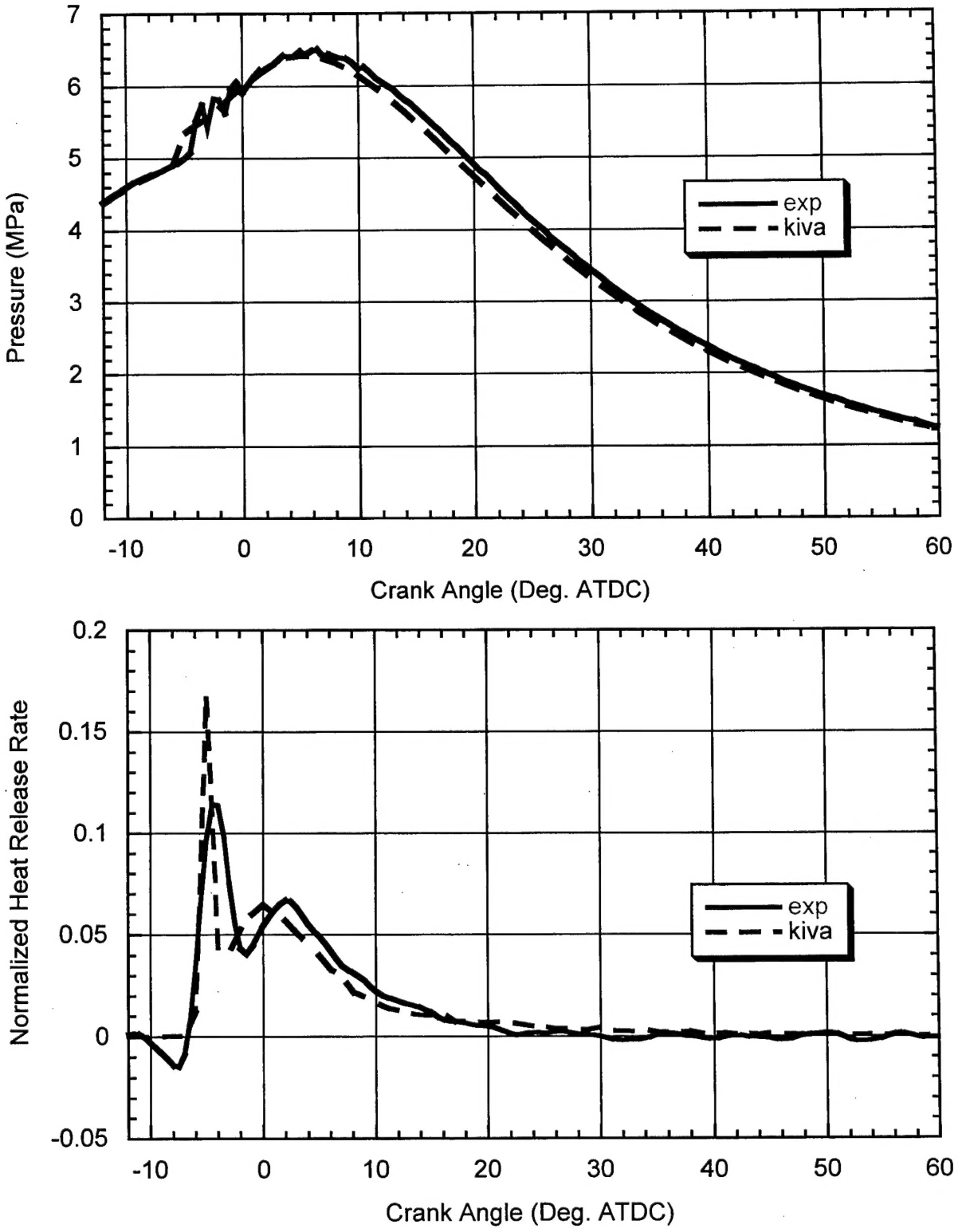

Figure 3: Comparison of coherent flamelet model with results for the Sandia engine (global equivalence ratio of 0.25).

References

Candel, S.M., Darabiha, N., Esposito, E., Giovangigli, V., Lacas, F., Laverdant, A., Maistret, E., Poinsot, T., Trouve, A., Veynante, D., & Zikikout, S., 1988, "Coherent Flame Modelling of Turbulent Reacting Flows," Laboratoire E.M2.C. du C.N.R.S. et de I'E.C.P., Chatenay-Malabry, France.

Kong, S.-C., and Reitz, R.D., 1993, "Multidimensional Modeling of Diesel Ignition and Combustion Using A Multistep Kinetics Models," ASME Transactions, Journal of Engineering for Gas Turbines and Power, Paper 93-ICE-22 115, No. 4, pp. 781-789

Marble, F.E. & Broadwell, J.E., 1977, "The coherent flame model for turbulent chemical reactions," Project Squid Report TRW-9-PU.

Musculus, M.P. & Rutland, C.J., 1995, "Coherent Flamelet Modeling of Diesel Engine Combustion," Combustion Science & Technology, 104, 4-6, pp. 295-337.

REPORT OF INVENTIONS

"Fuel Injector Nozzle with Tangential Orifices" Ali Ulidogan – Caterpillar, P.O. Box 740, Pontiac, IL 61764 and Rolf Reitz, Engine Research Center